

Electron and Muon Anomalous Magnetic Moments in the Inverse Seesaw Extended NMSSM

Junjie Cao, Yangle He, Jingwei Lian, Di Zhang and Pengxuan Zhu

Department of Physics, Henan Normal University, 453007, China

E-mail: junjiecao@alumni.itp.ac.cn, heyangle@htu.edu.cn,
ljwfly@hotmail.com, dz481655@gmail.com, zhupx99@icloud.com

ABSTRACT: The recently improved observation of the fine structure constant has led to a negative 2.4σ anomaly of electron $g-2$. Combined with the long-existing positive 3.7σ discrepancy of the muon anomalous magnetic moment, it is interesting and difficult to explain these two anomalies with a consistent model without introducing flavor violations. We show that they can be simultaneously explained in the inverse seesaw extended next-to-minimal supersymmetric standard model (ISS-NMSSM) by the Higgsino-sneutrino contributions to $(g-2)_e$ and $(g-2)_\mu$. The spectrum features prefer light μ , which can predict m_Z naturally, and it is not difficult to obtain a τ -type sneutrino dark matter candidate that is compatible with the observed dark matter relic density and the bounds from dark matter direct detection experiments. Due to the compressed spectra and the undetectable decay mode of selectrons, they can evade the current Large Hadron Collider (LHC) constraints.

Contents

1	Introduction	1
2	Inverse seesaw mechanism extended next-to-minimal supersymmetric standard model (ISS-NMSSM) and the lepton $g - 2$	4
2.1	Brief introduction to inverse seesaw next-to-minimal supersymmetric standard model (ISS-NMSSM)	4
2.2	Lepton anomalous magnetic moment in ISS-NMSSM	6
3	Features of combined explanation to Δa_e and Δa_μ in ISS-NMSSM	8
4	Dark matter phenomenology	16
4.1	Sneutrino dark matter	16
4.2	Effect of dark matter embedding on sparticle signal at the Large Hadron Collider (LHC)	17
5	Constraints from LHC sparticle searches	19
6	Summary	25
A	Validations of LHC analyses	26

1 Introduction

Since Schwinger showed that $a_\ell \equiv (g_\ell - 2)/2 = \frac{\alpha}{2\pi}$ [1], the anomalous magnetic moments of charged leptons have survived rigorous tests of the quantum electrodynamics (QED) and the later Standard Model (SM) of particle physics for more than half a century. Recently, an improvement of the measurement of the fine structure constant α , via the recoil frequency of cesium-133 atoms, has yielded the most accurate measurement [2]:

$$\alpha^{-1}(\text{Cs}) = 137.035999046(27). \quad (1.1)$$

As a result, there is a negative 2.4σ discrepancy between the theoretical prediction a_e^{SM} [3] and the existing experimental measurement a_e^{exp} [4, 5] of the electron anomalous magnetic moment,

$$\Delta a_e \equiv a_e^{\text{exp}} - a_e^{\text{SM}} = (-87 \pm 36) \times 10^{-14}. \quad (1.2)$$

Meanwhile, the long-standing discrepancy of the muon anomalous magnetic moment [6] between the SM prediction a_μ^{SM} [6–14] and the observed value in the E821 experiment of Brookhaven National Laboratory (BNL) a_μ^{exp} [15] is

$$\Delta a_\mu \equiv a_\mu^{\text{exp}} - a_\mu^{\text{SM}} = (279 \pm 76) \times 10^{-11}, \quad (1.3)$$

corresponding to a 3.7σ discrepancy.

There is insufficient evidence to show that these two anomalies are indeed signs of new physics (NP). The Discovery level confirmation of Δa_μ , for example, requires efforts from the currently running E989 experiment at the Fermilab and the future J-PARC experiment and also progress in reducing the theoretical uncertainty. Providing a common explanation to these two anomalies in an NP model is very challenging. In general, in a complete renormalizable model, a_ℓ can only be a quantum loop effect, because it comes from a dimension-5 operator. In a generic NP model without flavor violation, the new contribution to the anomalous magnetic moment a_ℓ^{NP} is proportional to the mass square of the lepton times an NP factor R_ℓ^{NP} . Taking the central values of the two anomalies in Eq. (1.1) and (1.2), one can easily find that there needs to be a difference of about -14 between R_e^{NP} and R_μ^{NP} ,

$$\frac{R_e^{\text{NP}}}{R_\mu^{\text{NP}}} = \frac{m_\mu^2 \Delta a_e}{m_e^2 \Delta a_\mu} \sim -14, \quad (1.4)$$

which is difficult to achieve from a common physical origin.

At present, there have already been several discussions offering combined explanations of the experimental results for electron and muon anomalous magnetic moments [16–46]. Among these discussions, the supersymmetry (SUSY) framework includes a chiral enhancement factor $\tan \beta$, which has shown promising results [34]. Ref. [16] argued that the combined explanation in the SUSY framework needs relatively large non-universal trilinear A -terms and also requires a flavor violation (for a more detailed discussion, see Ref. [47] and [35]). Due to the constraint from the lepton flavor violating process, Ref. [33] examined the minimal flavor violation within the minimal supersymmetric standard model (MSSM) and found its compatibility with the Higgs mediation scenario. However, since the value of parameter μ needs to be at $\mathcal{O}(100 \text{ TeV})$, the parameter space of the explanation in Ref. [33] is unattractive.

More recently, Ref. [30] argued that in the MSSM without any flavor violation, a combined explanation can be achieved by setting the conditions that $\text{sgn}(M_1 \mu) < 0$ and $\text{sgn}(M_2 \mu) > 0$. The corresponding result features very light selectrons and wino-like charginos, which avoid the Large Hadron Collider (LHC) constraint due to their degenerate spectra. The solution of Ref. [30] is impressive, but it also has two unsatisfactory characteristics. One is that the solution prefers heavy Higgsinos with masses $\mu \sim \mathcal{O}(1 \text{ TeV})$. This leads to a relatively fine-tuned electroweak sector. In general, μ should be close to the Z boson mass m_Z to avoid large cancellation when

predicting the observed value of $m_Z = 91.2$ GeV [48–52]. $\mu \sim 1$ TeV often induces tuning on the order of $1/10000$ to predict m_Z . The other is that wino-like particles are too light due to the current restrictions of the LHC direct SUSY searches. The wino exclusion planes reported by ATLAS and CMS within the simplified model framework are appropriate for the scenario of Ref. [30]. According to Fig. 8 in the CMS report [53], for example, the benchmark points in Ref. [30] with $M_2 \sim 200$ GeV are on the verge of being excluded by the multi-lepton plus E_T^{miss} signal via the electroweakino channel $pp \rightarrow \tilde{\chi}_1^\pm \tilde{\chi}_2^0$.

In our previous work [54], we investigated the observation that in the inverse-seesaw mechanism extended next-to-minimal supersymmetric standard model (ISS-NMSSM), due to the $\mathcal{O}(0.1)$ level Yukawa coupling Y_ν of the Higgs field to the right-handed neutrino, the Higgsino–sneutrino (HS) loop can be a new source of a_μ to explain Δa_μ . Unlike the MSSM, the newly introduced HS contribution a_ℓ^{HS} in the ISS-NMSSM prefers a light μ . The sign of a_ℓ^{HS} is determined by the kinematic mixing of sneutrino fields $\tilde{\nu}_L^\ell$, $\tilde{\nu}_R^\ell$, and $\tilde{\nu}_x^\ell$ for a given flavor ℓ , not by the mixing of charginos or neutralinos. In the ISS-NMSSM explanation, the masses of wino-like particles can be much heavier than the current LHC bounds. One can also assume one generation of sneutrinos to be the lightest supersymmetric particles (LSPs), which act as a dark matter (DM) candidate co-annihilating with Higgsinos to achieve the observed relic density. Due to the singlet nature, the DM-nucleus scattering cross section is naturally suppressed below the current experimental detection limits [54–56]. In this case, the neutral Higgsinos are the next-to-lightest supersymmetric particles (NLSPs) that decay into the invisible final states of the collider ($\tilde{H}^0 \rightarrow \nu\bar{\nu}$). The charged Higgsino decays into a soft charged lepton and DM ($\tilde{H}^\pm \rightarrow \ell^\pm \tilde{\nu}$). Due to the lower production rate than that of winos and the degenerate mass spectrum, the current LHC data still allow a low Higgsino mass of around 100 GeV. Thus, compared with the MSSM framework, the ISS-NMSSM is more natural for providing common explanations for Δa_e and Δa_μ .

In this work, we investigate this issue by applying the ISS-NMSSM to explain Δa_e and Δa_μ . The remainder of this paper is organized as follows. First, we briefly introduce the ISS-NMSSM and the properties of leptonic $g-2$ in Section 2. We then scan the parameter space that explains both the electron and muon $g-2$ discrepancies and analyze the characteristics of the input parameters and particle mass spectrum in Section 3. In Section 4, we find that our scenario can be embedded into a τ -type sneutrino, which co-annihilates with a Higgsino to achieve the observed DM relic density and does not conflict with the current DM direct search observations. In Section 5, we show the impact of the current LHC SUSY particle direct searches. Finally, we draw conclusion in Section 6.

2 Inverse seesaw mechanism extended next-to-minimal supersymmetric standard model (ISS-NMSSM) and the lepton $g - 2$

2.1 Brief introduction to inverse seesaw next-to-minimal supersymmetric standard model (ISS-NMSSM)

The complete definition of the ISS-NMSSM Lagrangian, such as quantum number setting, can be found in Ref. [57]. Here, we only briefly introduce the basic idea of the ‘inverse-seesaw’ extension and the neutrino sector.

The ‘inverse-seesaw’ mechanism is added to the NMSSM framework by introducing two gauge singlet superfields $\hat{\nu}$ and \hat{X} with opposite lepton numbers $L = -1$ and $L = 1$, respectively. With the assumptions of R -parity conservation, not introducing the $\Delta L = 1$ lepton number violation, the superpotential W is given as follows:

$$W = Y_u \hat{Q} \cdot \hat{H}_u \hat{u} + Y_d \hat{H}_d \cdot \hat{Q} \hat{d} + Y_e \hat{H}_d \cdot \hat{L} \hat{e} + \lambda \hat{S} \hat{H}_u \cdot \hat{H}_d + \frac{\kappa}{3} \hat{S}^3 + \frac{1}{2} \mu_X \hat{X} \hat{X} + \lambda_N \hat{S} \hat{\nu} \hat{X} + Y_\nu \hat{L} \cdot \hat{H}_u \hat{\nu}. \quad (2.1)$$

The first line of Eq. (2.1) is the standard NMSSM superpotential. The soft breaking terms of the ISS-NMSSM are given as follows:

$$V_{\text{soft}} = V_{\text{NMSSM}} + M_\nu^2 \tilde{\nu}_R \tilde{\nu}_R^* + M_X^2 \tilde{x} \tilde{x}^* + \left(\frac{1}{2} B_{\mu_X} \tilde{x} \tilde{x} + \lambda_N A_N S \tilde{\nu}_R^* \tilde{x} + Y_\nu A_\nu \tilde{\nu}_R^* \tilde{L} \cdot H_u + \text{h.c.} \right), \quad (2.2)$$

where V_{NMSSM} is the NMSSM soft breaking term, and $\tilde{\nu}_R$ and \tilde{x} are the scalar parts of superfields $\hat{\nu}$ and \hat{X} , respectively. The dimensional parameter μ_X is a small X -type neutrino mass term, which often is treated as an effective mass parameter to obtain the tiny masses of active neutrinos. The introduction of μ_X violates the lepton number due to the $\Delta L = 2$ term $\mu_X \hat{X} \hat{X}$ and the \mathbb{Z}_3 symmetry of the superpotential. Numerically, both μ_X and the soft mass term B_{μ_X} are extremely small, and they slightly split the complex sneutrino field into the CP -even part and the CP -odd part. In the numerical calculation of a_ℓ , the influence of these two non-vanishing parameters can be ignored. For simplicity, we simply set their value to zero.¹ In this

¹Actually, μ_X can be determined by the active neutrino experimental data and other parameters, which is discussed elsewhere [58, 59], as follows:

$$\mu_X = M_R^T m_D^{T-1} U_{\text{PMNS}}^* m_\nu^{\text{diag}} U_{\text{PMNS}}^\dagger m_D^{-1} M_R, \quad (2.3)$$

where $m_D = \frac{1}{\sqrt{2}} Y_\nu v_u$ and $M_R = \frac{1}{\sqrt{2}} \lambda_N v_s$ are the 3×3 neutrino Dirac mass matrices, and U_{PMNS} is the Pontecorvo–Maki–Nakagawa–Sakata (PMNS) matrix extracted from low-energy experiments [6].

work, all the non-SM parameters, such as Y_ν , λ_N , and A_N , are flavor diagonal. That is, there are no flavor mixing parameters.

The SUSY particles of particular importance to a_ℓ are sleptons $\tilde{\ell}$, ℓ -type sneutrinos, neutralinos $\tilde{\chi}_i^0$, and charginos $\tilde{\chi}_i^\pm$. The neutralino and chargino sector in the ISS-NMSSM were same as that of the NMSSM. On the basis of $\phi^0 = (\tilde{B}, \tilde{W}^3, \tilde{H}_d^0, \tilde{H}_u^0, \tilde{S})^T$, the symmetric neutralino mixing matrix \mathcal{M}_0 is as follows:

$$\mathcal{M}^0 = \begin{pmatrix} M_1 & 0 & -\frac{g_1}{\sqrt{2}}v_d & \frac{g_1}{\sqrt{2}}v_u & 0 \\ & M_2 & \frac{g_2}{\sqrt{2}}v_d & -\frac{g_2}{\sqrt{2}}v_u & 0 \\ & & 0 & -\mu & -\lambda v_u \\ & & & 0 & -\lambda v_d \\ & & & & 2\kappa v_s \end{pmatrix}, \quad (2.4)$$

where the Higgsino mass $\mu = \lambda v_s$ is an effective μ -term after the electroweak symmetry breaking, and v_u , v_d , and v_s represent the vacuum expectation values (vevs) of the Higgs field H_u , H_d , and S , respectively. The mass eigenstates $\tilde{\chi}_i^0 = N_{ij}\phi_j^0$ are arranged in ascending order of mass. With the basis $\phi^+ = (\tilde{W}^+, \tilde{H}_u^+)$ and $\phi^- = (\tilde{W}^-, \tilde{H}_d^-)$, the chargino mass term is given by $\phi^- \mathcal{M}^\pm \phi^+ + h.c.$ with the mass matrix

$$\mathcal{M}^\pm = \begin{pmatrix} M_2 & g_2 v_u \\ g_2 v_d & \mu \end{pmatrix}. \quad (2.5)$$

The corresponding mass eigenstates are defined by

$$\tilde{\chi}_i^+ = V_{ij}\phi_j^+, \quad \tilde{\chi}_i^- = U_{ij}\phi_j^-. \quad (2.6)$$

The symmetric mass matrix \mathcal{M}_ℓ^2 for slepton $\tilde{\ell}$ for each flavor ℓ in the $(\tilde{\ell}_L, \tilde{\ell}_R)$ basis is

$$\mathcal{M}_\ell^2 = \begin{pmatrix} M_{L_\ell}^2 + m_\ell^2 + m_Z^2 \cos 2\beta (\sin^2 \theta_W - \frac{1}{2}) & m_\ell (A_{E_\ell} - \mu \tan \beta) \\ M_{E_\ell}^2 - \sin^2 \theta_W m_Z^2 \cos 2\beta & \end{pmatrix}, \quad (2.7)$$

and the corresponding rotation matrix is represented by X^ℓ .

In terms of the particle composition, the ISS-NMSSM differs from the NMSSM [60] only in the neutrino sector. In the neutrino part, the observation on the unitarity of active neutrino mass rotation matrix can be derived from the non-diagonality of μ_X . As a result, the unitary constraint can be read in a flavor diagonal form,

$$\frac{\lambda_{N_e}}{Y_{\nu_e}} \frac{\mu}{\lambda v_u} > 14.1, \quad \frac{\lambda_{N_\mu}}{Y_{\nu_\mu}} \frac{\mu}{\lambda v_u} > 33.7, \quad \frac{\lambda_{N_\tau}}{Y_{\nu_\tau}} \frac{\mu}{\lambda v_u} > 9.4. \quad (2.8)$$

These inequalities indicate that, for given λ_N and the Higgs sector parameters λ , $\tan \beta$, and μ , this unitary constraint allows Y_{ν_e} to be greater than Y_{ν_μ} , which is good for explaining Δa_e . For each generation $\ell = e, \mu, \tau$, the sneutrino fields are the mixtures of left-handed sneutrino $\tilde{\nu}_L^\ell$, right-handed sneutrino $\tilde{\nu}_R^\ell$, and x -type

sneutrino $\tilde{\nu}_x^\ell$. On the basis of $\phi_\nu^\ell = (\tilde{\nu}_L^\ell, \tilde{\nu}_R^\ell, \tilde{\nu}_x^\ell)$, the symmetric mass matrix \mathcal{M}_ν^2 is given by

$$\mathcal{M}_\nu^2 = \frac{1}{2} \begin{pmatrix} 2M_{L_\ell}^2 + Y_{\nu_\ell}^2 v_u^2 + m_Z^2 \cos 2\beta & Y_{\nu_\ell}(\sqrt{2}A_{\nu_\ell}v_u - \lambda v_d v_s) & Y_{\nu_\ell} \lambda_{N_\ell} v_u v_s \\ & 2M_{\nu_\ell}^2 + Y_{\nu_\ell}^2 v_u^2 + \lambda_{N_\ell}^2 v_s^2 & \lambda_{N_\ell}(\sqrt{2}A_{N_\ell}v_s + \kappa v_s^2 - \lambda v_u v_d) \\ & & 2M_{X_\ell}^2 + \lambda_{N_\ell}^2 v_s^2 \end{pmatrix}. \quad (2.9)$$

The mass eigenstate of one generation sneutrino is $\tilde{\nu}_i^\ell = \sum_j Z_{ij}^\ell \phi_{\nu,j}^\ell$, with Z^ℓ denoting the unitary matrix to diagonalize \mathcal{M}_ν^2 . From Eq. (2.9), one can easily find that the diagonal elements can be adjusted by the soft breaking parameters $M_{L_\ell}^2$, $M_{\nu_\ell}^2$, and $M_{X_\ell}^2$. For the off-diagonal elements, Higgs vev terms, such as $Y_{\nu_\ell} v_u$ and $\lambda_{N_\ell} v_s$, provide a scale for the mixing of the three fields of left-handed, right-handed, and x -type sneutrinos. The relative signs and the magnitude of different sneutrino components can be adjusted by two A -term soft breaking parameters A_{ν_ℓ} and A_{N_ℓ} .

2.2 Lepton anomalous magnetic moment in ISS-NMSSM

The lepton anomalous magnetic moment a_ℓ always corresponds to lepton chirality-flipping interactions. In the ISS-NMSSM, the chirality of the ℓ -lepton number can be flipped by Y_{e_ℓ} or Y_{ν_ℓ} . All the SM-like diagrams (the ℓ -lepton number is carried only by lepton ℓ and/or neutrino ν_ℓ) involve only SM-particles, so their contribution to a_ℓ is identical to the SM prediction a_ℓ^{SM} . Therefore, the SUSY contribution a_ℓ^{SUSY} , in which the ℓ -lepton number is carried also by a scalar lepton $\tilde{\ell}$ and/or ℓ -type sneutrino $\tilde{\nu}_\ell$, provides the source of the observed anomaly Δa_ℓ .

The one-loop SUSY contribution to a_ℓ in the ISS-NMSSM is given as follows:

$$\begin{aligned} a_\ell^{\text{SUSY}} &= a_{\tilde{\chi}^0 \tilde{\ell}} + a_{\tilde{\chi}^\pm \tilde{\nu}}, \\ a_{\tilde{\chi}^0 \tilde{\ell}} &= \frac{m_\ell}{16\pi^2} \sum_{i,l} \left\{ -\frac{m_\ell}{12m_{\tilde{\ell}_l}^2} (|n_{il}^L|^2 + |n_{il}^R|^2) F_1^N(x_{il}) + \frac{m_{\tilde{\chi}_i^0}}{3m_{\tilde{\ell}_l}^2} \text{Re}(n_{il}^L n_{il}^R) F_2^N(x_{il}) \right\}, \\ a_{\tilde{\chi}^\pm \tilde{\nu}} &= \frac{m_\ell}{16\pi^2} \sum_{j,n} \left\{ \frac{m_\ell}{12m_{\tilde{\nu}_{\ell,n}}^2} (|c_{jn}^L|^2 + |c_{jn}^R|^2) F_1^C(x_{jn}) + \frac{2m_{\tilde{\chi}_j^\pm}}{3m_{\tilde{\nu}_{\ell,n}}^2} \text{Re}(c_{jn}^L c_{jn}^R) F_2^C(x_{jn}) \right\}. \end{aligned} \quad (2.10)$$

Here, $i = 1, \dots, 5$ and $j = 1, 2$ respectively denote the neutralino and chargino indices, $l = 1, 2$ denotes the slepton index, $n = 1, 2, 3$ denotes the sneutrino index, and

$$\begin{aligned} n_{il}^L &= \frac{1}{\sqrt{2}} (g_2 N_{i2} + g_1 N_{i1}) X_{l1}^{\ell,*} - Y_{e_\ell} N_{i3} X_{l2}^{\ell,*}, \quad n_{il}^R = \sqrt{2} g_1 N_{i1} X_{l2}^\ell + Y_{e_\ell} N_{i3} X_{l1}^\ell, \\ c_{jn}^L &= -g_2 V_{j1} Z_{n1}^{\ell,*} + Y_{\nu_\ell} V_{j2} Z_{n2}^{\ell,*}, \quad c_{jn}^R = Y_{e_\ell} U_{j2} Z_{n1}^\ell. \end{aligned} \quad (2.11)$$

The kinematic loop function $F(x)$ is normalized with condition $F(1) = 1$, which is given as follows:

$$\begin{aligned}
F_1^N(x) &= \frac{2}{(1-x)^4} (1 - 6x + 3x^2 + 2x^3 - 6x^2 \ln x), \\
F_2^N(x) &= \frac{3}{(1-x)^3} (1 - x^2 + 2x \ln x), \\
F_1^C(x) &= \frac{2}{(1-x)^4} (2 + 3x - 6x^2 + x^3 + 6x \ln x), \\
F_2^C(x) &= -\frac{3}{2(1-x)^3} (3 - 4x + x^2 + 2 \ln x),
\end{aligned} \tag{2.12}$$

with definitions $x_{il} \equiv m_{\tilde{\chi}_i^0}^2/m_{\tilde{\ell}_l}^2$ and $x_{jn} \equiv m_{\tilde{\chi}_j^\pm}^2/m_{\tilde{\nu}_n}^2$.

We compare the differences between the MSSM contribution and the ISS-NMSSM contribution with a_ℓ . The full expression of a_ℓ^{SUSY} in the MSSM is very similar to that in the ISS-NMSSM; the difference is that c^L in Eq. (2.11) of MSSM does not contain the $Y_{\nu_\ell} V_{j2}$ term [61]. There are two main reasons that it is difficult for the MSSM to explain the two anomalies Δa_μ and Δa_e . The first reason is that most of the relevant parameters are irrelevant to the lepton flavor. The parameter μ governs the Higgsino $\tilde{H}_u - \tilde{H}_d$ transition and the dominant part of the scalar lepton mixing term, so that all the contributions acquire a common factor $\mu \tan \beta$. Other parameters, e.g., M_1 and M_2 , affect the sign of the corresponding contributions in a_ℓ^{SUSY} . Compared with $\mu \tan \beta$, the trilinear soft parameter A_e is usually ignored in the left-handed and right-handed scalar lepton mass mixing. Thus, in general, a_e^{SUSY} and a_μ^{SUSY} are highly correlated in the MSSM. The second reason is the correlation between $a_\ell^{\tilde{\chi}^0 \tilde{\ell}}$ and $a_\ell^{\tilde{\chi}^\pm \tilde{\nu}}$. In the MSSM, the mass of the left-handed slepton $\tilde{\ell}_L$ is slightly larger than the mass of sneutrino $\tilde{\nu}^\ell$ by about 15 GeV for large $\tan \beta$. As a result, the wino-Higgsino loop in $a_\ell^{\tilde{\chi}^0 \tilde{\ell}}$ is about $-1/2$ times that in $a_\ell^{\tilde{\chi}^\pm \tilde{\nu}}$.

In ISS-NMSSM, the correlation between the contributions coming from the chargino-sneutrino loop and from the neutralino-slepton loop is relatively weak. Moreover, the ISS-NMSSM contribution a_ℓ^{SUSY} includes an extra HS term, which is depicted in Fig. 1 via the mass insertion technique. Accordingly, this HS contribution a_ℓ^{HS} can be expressed as

$$a_\ell^{\text{HS}} \approx m_\ell^2 \times \frac{1}{48\pi^2 v} \frac{Y_{\nu_\ell}}{\mu \cos \beta} \left\{ \sum_n Z_{n1}^\ell Z_{n2}^\ell \times x_n F_2^C(x_n) \right\}, \quad x_n \equiv \frac{\mu^2}{m_{\tilde{\nu}_{\ell,n}}^2}, \tag{2.13}$$

where $v = \sqrt{v_u^2 + v_d^2} = 173$ GeV, and $x F_2^C(x)$ increases monotonically with x , with its value ranging from 0 to 1.5. Eq. (2.13) shows that a_ℓ^{HS} is enhanced by the factor $\cos \beta \approx 1/\tan \beta$ for large $\tan \beta$. A relatively large Y_{ν_ℓ} is expected to achieve a larger a_ℓ^{HS} . The lepton chirality flipping in the HS contribution is reflected in the left-right mixing term $Z_{n1} Z_{n2}$ for each sneutrino $\tilde{\nu}_n$. If the x -field-dominated sneutrino

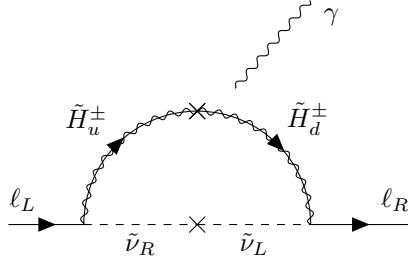


Figure 1. One-loop diagram of Higgsino-sneutrino contribution, the additional contribution to a_ℓ^{SUSY} in the inverse-seesaw mechanism extended next-to-minimal supersymmetric standard model (ISS-NMSSM) compared to the minimal supersymmetric standard model (MSSM).

is too heavy, the contribution from the left-handed dominated sneutrino and the right-handed dominated state to a_ℓ cancel each other because $Z_{11}^\ell Z_{12}^\ell \approx -Z_{21}^\ell Z_{22}^\ell$. As a result, the way to avoid this cancellation is to mix enough x -field components in one of the lighter sneutrinos. As shown in Eq. (2.9), the mixture of the x -field and other fields is dominated by $\lambda_N v_s$. A light μ is favored for large a_ℓ^{HS} , so the small λ at $\mathcal{O}(0.01)$ often has a larger a_ℓ^{HS} . However, the leptonic unitary condition in Eq. (2.8) also prefers λ to have small values. The most attractive property of the HS explanation is that the left-right mixing $Z_{n1} Z_{n2}$ is positively related to A_ν . The magnitude and sign of the HS contribution can be adjusted by A_ν . Numerically, an $|A_\nu|$ at $\mathcal{O}(100 \text{ GeV})$ to $\mathcal{O}(1 \text{ TeV})$ is sufficient for a_ℓ^{HS} to explain both anomalies.

3 Features of combined explanation to Δa_e and Δa_μ in ISS-NMSSM

The relevant SUSY particle masses have different contributions to a_ℓ^{SUSY} . To reveal the detailed features of a_ℓ^{SUSY} in the ISS-NMSSM, which is covered up by the complexity of the loop functions $F(x)$ in Eq. (2.12), we use the `MultiNest` technique [62, 63] to scan the ISS-NMSSM parameter space with the following parameter values and ranges:

$$\begin{aligned}
& 0 < \lambda < 0.7, \quad |\kappa| < 0.7, \quad 100 \text{ GeV} < \mu < 500 \text{ GeV}, \quad \tan \beta = 60, \\
& A_\lambda = 2 \text{ TeV}, \quad -1 \text{ TeV} < A_\kappa < 1 \text{ TeV}, \quad -5 \text{ TeV} < A_t = A_b < 5 \text{ TeV}, \\
& |M_1| < 1 \text{ TeV}, \quad |M_2| < 1.5 \text{ TeV}, \\
& 100 \text{ GeV} < M_{L_e} < 1 \text{ TeV}, \quad 100 \text{ GeV} < M_{E_e} < 1 \text{ TeV}, \quad A_{E_e} = 0 \\
& 0 < Y_{\nu_e} < 0.8, \quad |A_{\nu_e}| < 2 \text{ TeV}, \quad 0 < \lambda_{N_e} < 0.8, \quad |A_{N_e}| < 2 \text{ TeV}, \\
& |M_{\nu_e}^2| < 1 \text{ TeV}^2, \quad |M_{X_e}^2| < 1 \text{ TeV}^2, \\
& 100 \text{ GeV} < M_{L_\mu} < 1 \text{ TeV}, \quad 100 \text{ GeV} < M_{E_\mu} < 1 \text{ TeV}, \quad A_{E_\mu} = 0 \\
& 0 < Y_{\nu_\mu} < 0.8, \quad |A_{\nu_\mu}| < 2 \text{ TeV}, \quad 0 < \lambda_{N_\mu} < 0.8, \quad |A_{N_\mu}| < 2 \text{ TeV}, \\
& |M_{\nu_\mu}^2| < 1 \text{ TeV}^2, \quad |M_{X_\mu}^2| < 1 \text{ TeV}^2,
\end{aligned} \tag{3.1}$$

where all parameters are defined at the scale of 1 TeV. All the other soft breaking parameters, like those first two generation squark, are fixed at a common value of 3 TeV. The prior probability distribution function (PDF) of these inputs are set as uniform distributions, and the n_{live} parameter, which indicates the number of the active points to determine the iso-likelihood contour in the **MultiNest** algorithm iteration, is set at 10000. The likelihood function χ^2 in the scan is taken as

$$\chi^2 = \chi_{a_\ell}^2 + \chi_{\text{Higgs}}^2 + \chi_{\text{veto}}^2, \tag{3.2}$$

where $\chi_{a_\ell}^2 = \frac{1}{2} \left(\frac{a_e^{\text{SUSY}} + 87 \times 10^{-14}}{36 \times 10^{-14}} \right)^2 + \frac{1}{2} \left(\frac{a_\mu^{\text{SUSY}} - 267 \times 10^{-11}}{76 \times 10^{-11}} \right)^2$ is a standard Gaussian form of two anomalies. χ_{Higgs}^2 requires the sample in the parameter space given by Eq. (3.1) to predict an SM-like Higgs boson compatible with current experimental observations using the **HiggsSignals-2.2.3** code [64–66] and to satisfy the constraints of a direct search of the Higgs boson using the **HiggsBounds-5.3.2** code [67]. χ_{veto}^2 is introduced to ensure that the LSP is a Higgsino, the electroweak vacuum is stable, sneutrino fields have not developed non-zero vevs, and the unitary constraint of Eq. (2.8) is satisfied.

In the numerical calculation, an ISS-NMSSM model file is generated by the **SARAH-4.14.3** package [68, 69], the particle spectra of the parameter samples are calculated by the **SPheno-4.0.3** [70, 71] and **FlavorKit** [72] packages, and electroweak vacuum stability and sneutrino stability are tested by the **Vevacious** [73, 74] package, in which the tunneling time from the input electroweak potential minimum to the true vacuum is obtained via the **CosmoTransitions** package [75].

The one-dimensional profile likelihood (PL) plots of $\chi_{a_\ell}^2$ with the values normalized to the maximum and marginal posterior probability density function (PDF) of the input parameters are shown in Fig. 2, 3, and 4. The value of PL for a fixed value of the parameter of interest, $\theta = \theta_0$, is the profiled value of nuisance parameters that maximized \mathcal{L} . Therefore, in a multi-dimensional model, the PL can be treated as

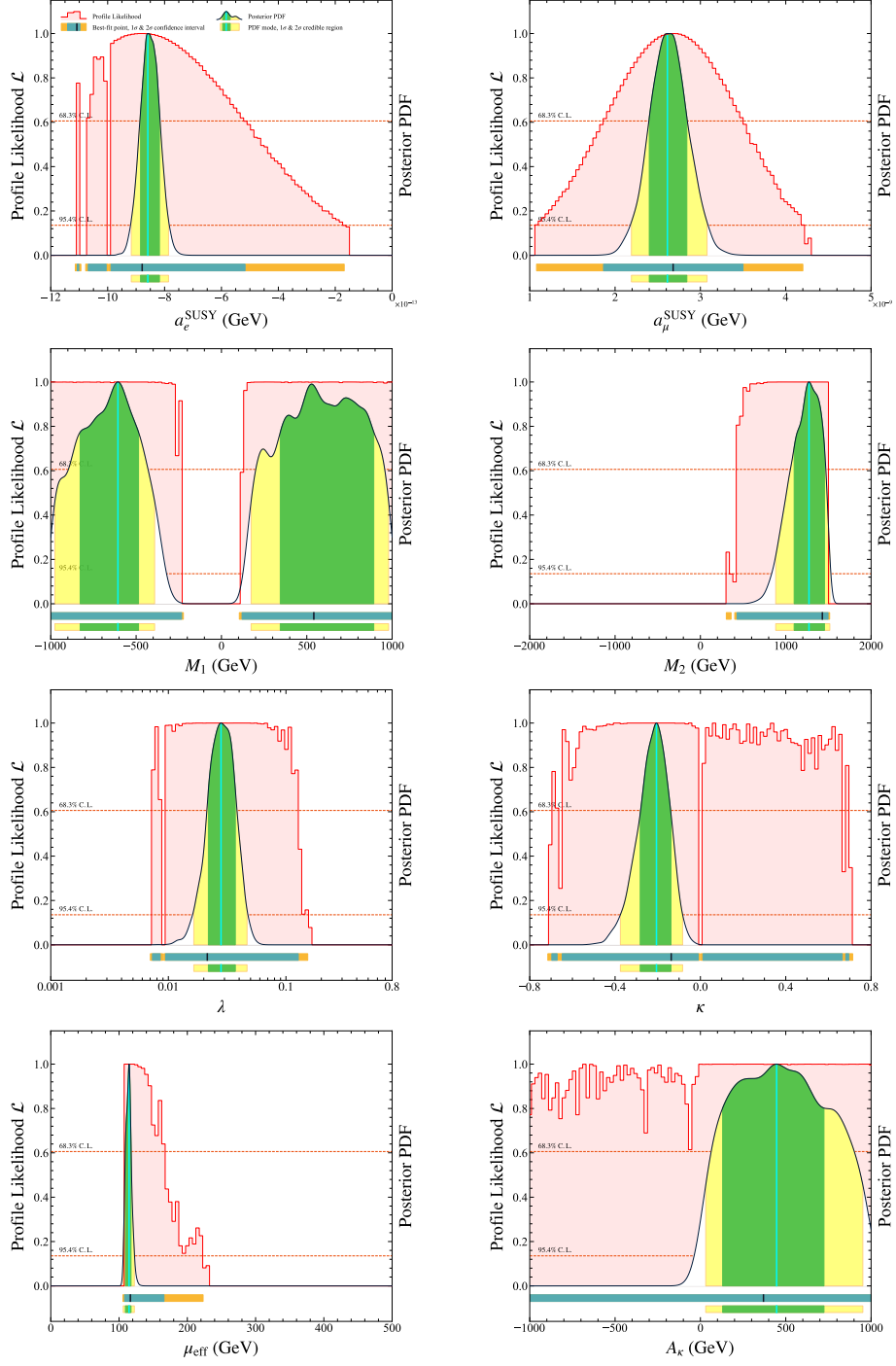


Figure 2. One-dimensional profile likelihood \mathcal{L} and posterior probability density function (PDF) distributions of a_ℓ^{SUSY} and electroweakino input parameters. Regions of orange areas colored blue show the 1σ (2σ) confidence interval, and the best-point is marked by a black vertical line. Regions of yellow areas colored green represent the 1σ (2σ) credible region.

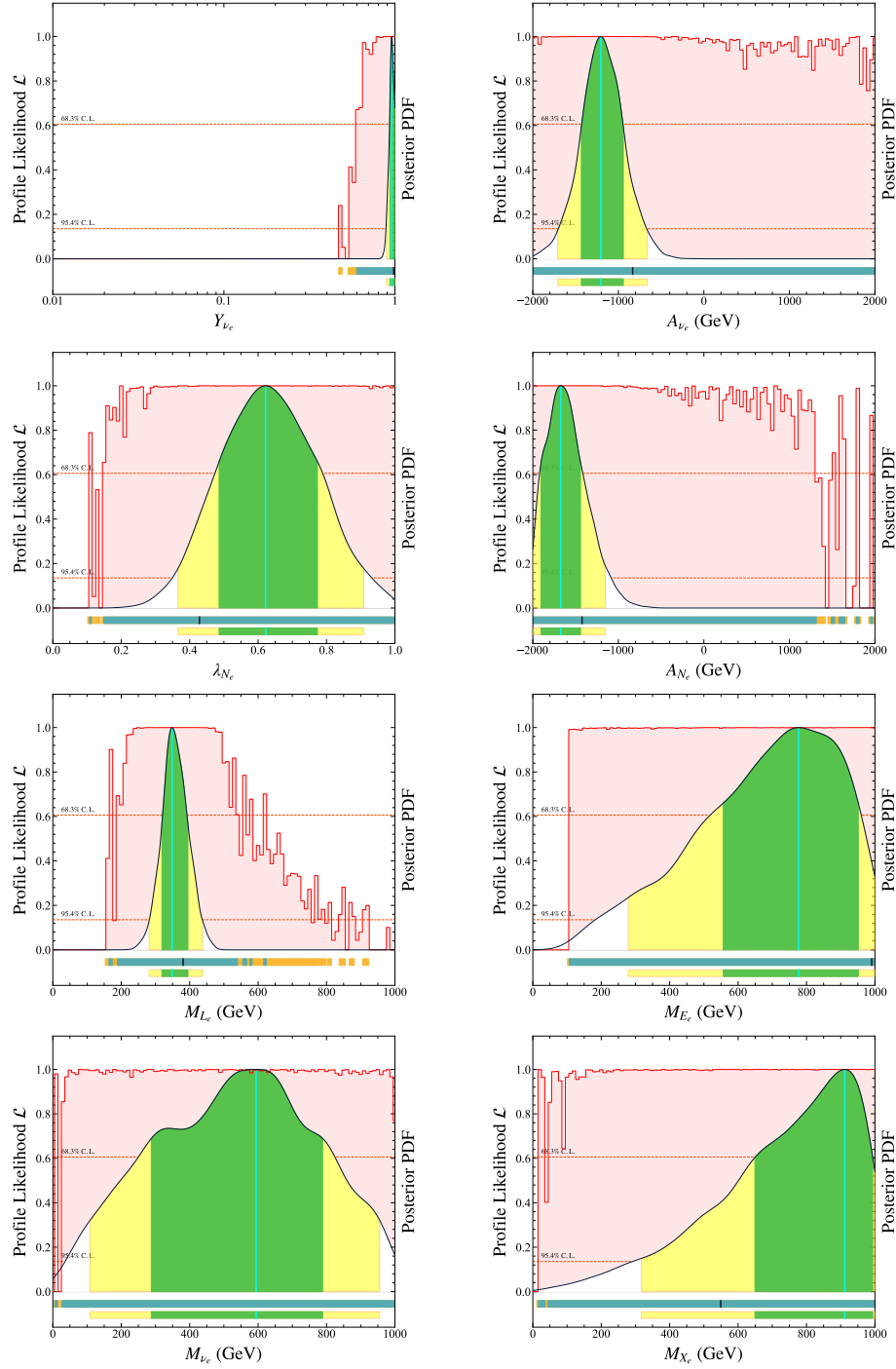


Figure 3. One-dimensional profile likelihood \mathcal{L} and posterior probability density function (PDF) distributions of the input parameters of e -type slepton and sneutrino. Regions of orange areas colored blue show the 1σ (2σ) confidence interval, and the best-point is marked by a black vertical line. Regions of yellow areas colored green represent the 1σ (2σ) credible region.

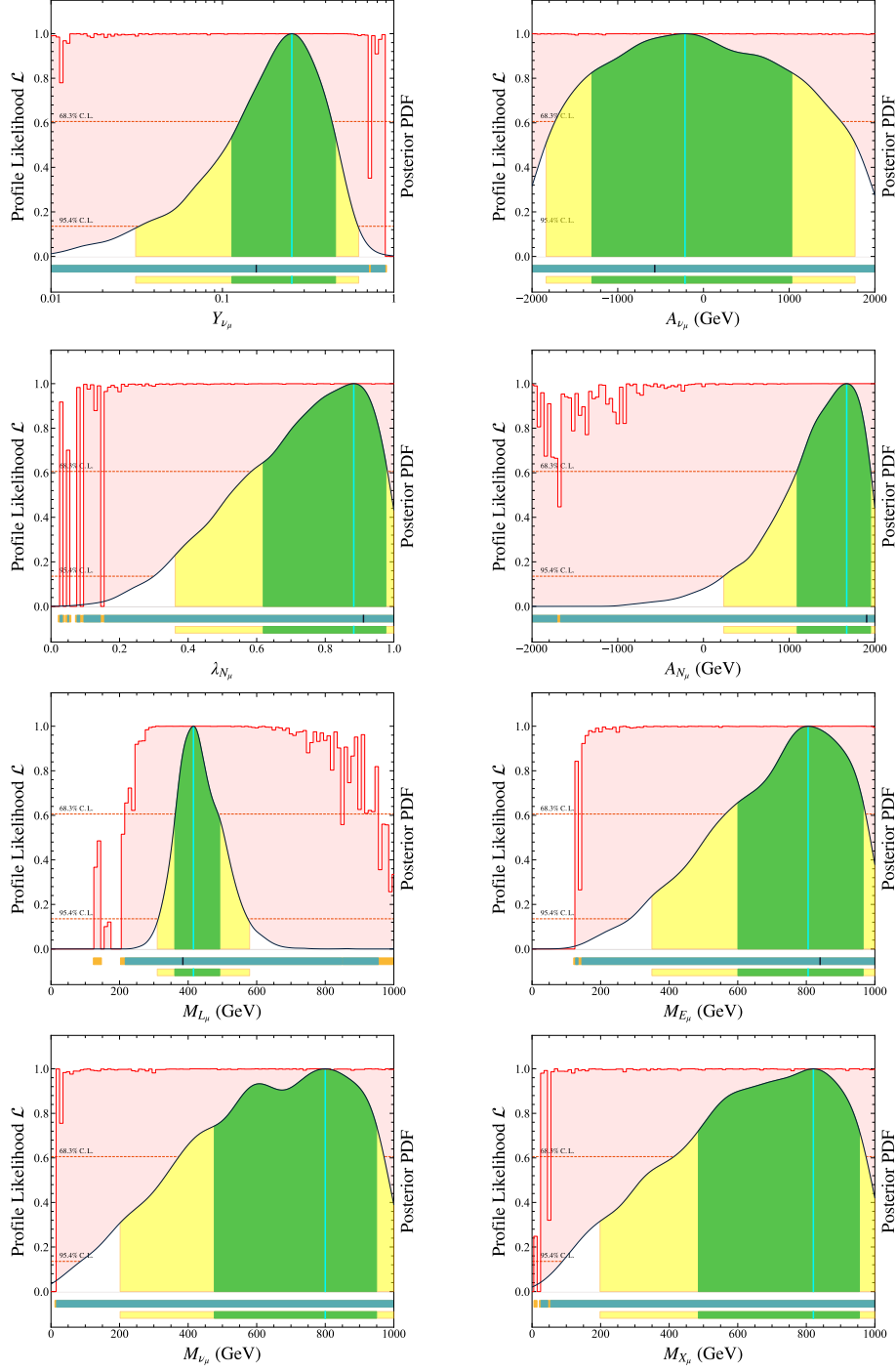


Figure 4. One-dimensional profile likelihood \mathcal{L} and posterior probability density function (PDF) distributions of the μ -flavor related input parameters. Regions of orange areas colored blue show the 1σ (2σ) confidence interval, and the best-point is marked by a black vertical line. Regions of yellow areas colored green represent the 1σ (2σ) credible region.

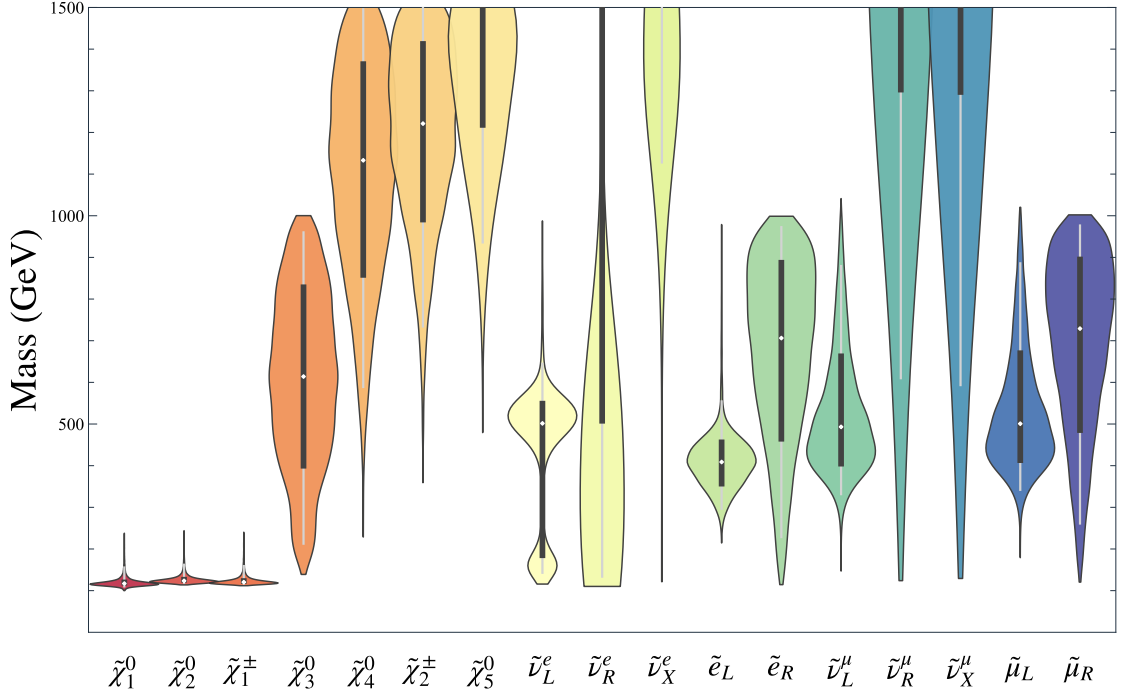


Figure 5. Violin plots showing the mass distributions of supersymmetry (SUSY) particles. Sleptons and sneutrinos are labeled by their dominated components. The violins are scaled by count. The thick vertical bar in the center indicates the interquartile range with the white dot representing the median, and the long vertical line represents the 95% confidence interval.

an indicator of how well the theory can explain the experiments in the subspace of $\theta = \theta_0$. Complementarily, the one-dimensional marginal posterior PDF reflects the volume of subspace $\theta = \theta_0$.

These figures show that ISS-NMSSM has a large parameter space to give a common explanation of Δa_e and Δa_μ . The results are summarized as follows:

- In the view of the PL, the smooth bell-shaped PL curves of a_e^{SUSY} and a_μ^{SUSY} indicate the ability of the ISS-NMSSM to fit the two anomalies. The missing part of the PL curve where $a_e^{\text{SUSY}} < -1 \times 10^{-12}$ indicates that a large a_e^{SUSY} is difficult to achieve in theory.
- The distributions of the input parameters M_2 , λ , μ , Y_{ν_e} , Y_{ν_μ} , and A_{ν_e} show some trends that verify the discussion in the previous section. The narrow PL picks of $100 \text{ GeV} \lesssim \mu \lesssim 150 \text{ GeV}$ and $Y_{\nu_e} \geq 0.7$ reflect the properties of Eq. (2.13) and the difficulty of explaining Δa_e . The wider credible region of the μ -type input parameter than that of e -type parameter also confirms this feature.

- For most input parameters, the credible regions are smaller than the confidence interval. The PL values are very close to 1 almost in the entire space. This implies that the value of these parameters are not affected by the two anomalies.
- $\mu \sim 110$ GeV and $0.015 \lesssim \lambda \lesssim 0.05$ cause the masses of all the singlet Higgs particles to be on the order of several TeV.
- M_1 and M_2 are often much greater than μ to reduce the correlations in the MSSM contributions to a_e^{SUSY} and a_μ^{SUSY} . The distributions of M_1 shows that the bino-slepton loop contribution is far from dominant. The distribution of M_2 shows that the wino-related contributions are suppressed in this explanation.

There were 8311 samples obtained that explained two anomalies within the 2σ range in total. In Fig. 5, we plot the mass distributions of the SUSY particles via violin plots², where sleptons and sneutrinos are labeled by their dominating components. The masses of the Higgsino triplets were around 110 GeV, and the wino particles were often heavier than 700 GeV. The masses of left-handed selectron \tilde{e}_L and $\tilde{\mu}_L$ were distributed around 400 GeV, and the right-handed sleptons were relatively heavy. In contrast to the MSSM spectrum, the mass of $\tilde{\nu}_L^e$ can be much lower than that of $\tilde{\nu}_R^e$ in the ISS-NMSSM.

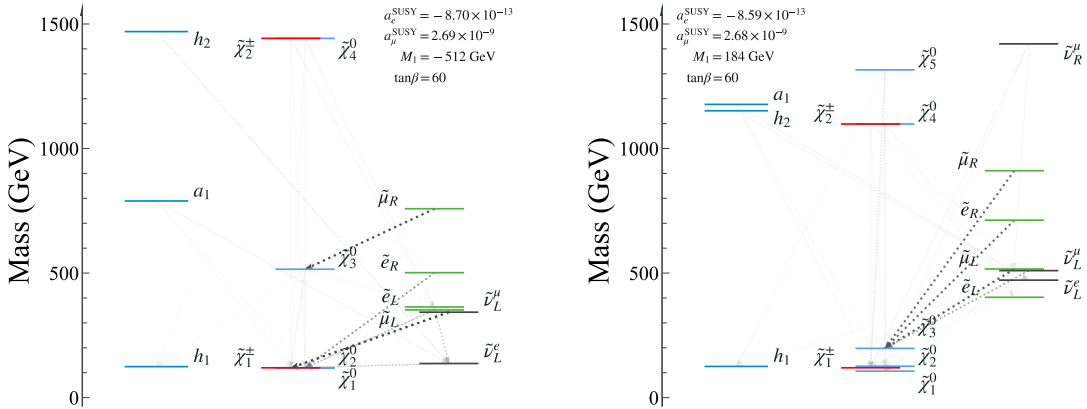


Figure 6. Higgs and sparticle spectra for the typical samples in the ISS-NMSSM. Sleptons and sneutrinos are labeled by their dominant components, the decay paths are shown with branching ratios $> 5\%$, and the widths of the lines are proportional to the branching ratios.

The Higgs and sparticle spectra for two typical parameter points are shown in Fig. 6. M_1 may play a crucial role in the mass splitting of Higgsinos. Taking the mixing terms as a perturbation and calculating the neutralino and chargino masses to the first order in perturbation theory, the mass splitting between Higgsinos are approximately given as follows:

²A violin plot is similar to a box plot; it shows the probability density smoothed by kernel density estimation [76].

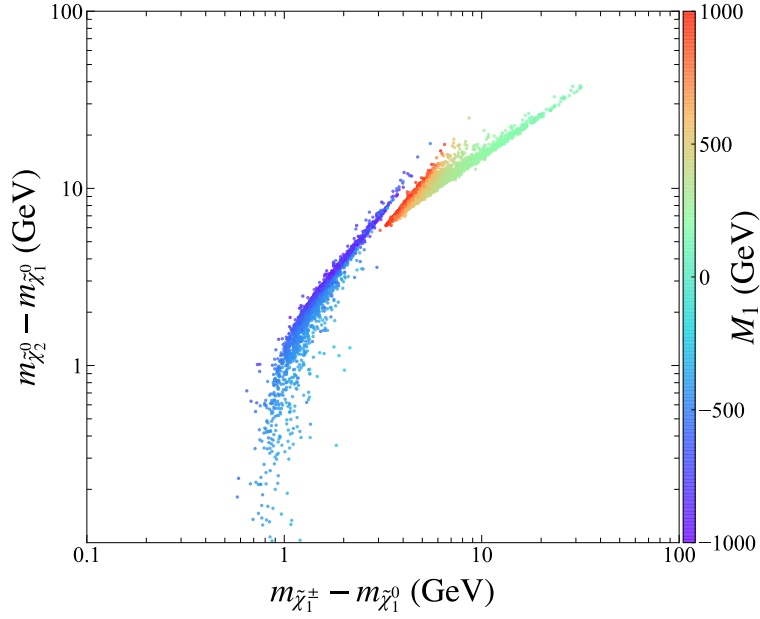


Figure 7. Mass splitting of Higgsinos for the scanned samples with the color bar indicating the value of M_1 .

$$\begin{aligned}
\Delta m(\tilde{\chi}_2^0, \tilde{\chi}_1^0) &\approx \left| \frac{g_1^2 v^2 (M_1 + \mu \sin 2\beta)}{2(M_1^2 - \mu^2)} + \frac{g_2^2 v^2 (M_2 + \mu \sin 2\beta)}{2(M_2^2 - \mu^2)} + \frac{\lambda^2 v^2 (m_{\tilde{S}} - \mu \sin 2\beta)}{m_{\tilde{S}}^2 - \mu^2} \right| \\
&\approx \left| \frac{g_1^2 v^2 M_1}{2(M_1^2 - \mu^2)} + \frac{g_2^2 v^2 M_2}{2(M_2^2 - \mu^2)} \right|, \\
\Delta m(\tilde{\chi}_1^\pm, \tilde{\chi}_1^0) &\approx \left| \frac{g_1^2 v^2 (1 + \sin 2\beta)}{2(M_1 - \mu)} + \frac{g_2^2 v^2 (1 + \sin 2\beta)}{2(M_2 - \mu)} + \frac{\lambda^2 v^2 (1 - \sin 2\beta)}{m_{\tilde{S}} - \mu} \right. \\
&\quad \left. + \frac{\lambda^2 (g_1^2 + g_2^2) v^4}{2(M_1 - \mu)(m_{\tilde{S}} - \mu)\mu} - \frac{g_2^2 v^2}{2\mu} \left(\frac{(m_2 \cos \beta + \mu \sin \beta)^2}{m_2^2 - \mu^2} - \cos^2 \beta \right) \right| \\
&\approx \left| \frac{g_1^2 v^2}{2(M_1 - \mu)} + \frac{g_2^2 v^2}{2(M_2 - \mu)} - \frac{g_2^2 v^2 \mu}{2(M_2^2 - \mu^2)} \right|,
\end{aligned} \tag{3.3}$$

where $m_{\tilde{S}} = 2\kappa v_s$ is the singlino mass. These formulae indicate that the effect of M_1 is negligibly small when $|M_1|$ is extremely large, while as it approaches zero from above (below), it can enhance (decrease) the splitting significantly. This characteristic is shown in Fig. 7, where we projected the scanned samples on the $\Delta m(\tilde{\chi}_1^\pm, \tilde{\chi}_1^0) - \Delta m(\tilde{\chi}_2^0, \tilde{\chi}_1^0)$ plane with the color bar denoting the M_1 value. This figure reveals that $\Delta m(\tilde{\chi}_1^\pm, \tilde{\chi}_1^0) \simeq 4$ GeV and $\Delta m(\tilde{\chi}_2^0, \tilde{\chi}_1^0) \simeq 10$ GeV when $|M_1| = 1$ TeV. When $M_1 \simeq 200$ GeV, the mass splittings increase to several tens of GeV, and when $M_1 \simeq -200$ GeV, they decrease to less than 1 GeV.

4 Dark matter phenomenology

In the ISS-NMSSM explanation of the two leptonic anomalous magnetic moments Δa_e and Δa_μ , the Higgsino mass is less than 200 GeV and acts as the LSP. Such a light Higgsino is not a good DM candidate, due to its spin-dependent and spin-independent scattering rates with nuclei larger than the current experimental limits [49, 77–81]. In the ISS-NMSSM, a right-handed-field- or x -field-dominated sneutrino can also serve as the DM candidate. The sizable neutrino Yukawa coupling Y_ν contributes significantly to the DM-nucleon scattering rate, so that e -type and μ -type sneutrinos cannot act as DM candidates. Fortunately, flavor mixing is forbidden in our model, and this enables us to take the lightest τ -type sneutrinos, $\tilde{\nu}_1^\tau$, and its charge conjugate state, $\tilde{\nu}_1^{\tau*}$, as feasible DM candidates [55–57]³. The candidates should be lighter than $\tilde{\chi}_1^0$ and dominated in components by the right-handed field $\tilde{\nu}_R$, the \tilde{x} -field, or their mixture. In addition, given the preferred parameters in the last section, one can further restrict their properties.

4.1 Sneutrino dark matter

First, we consider the annihilation of τ -type sneutrinos, whose thermally averaged cross-section at the freeze-out temperature should satisfy $\langle\sigma v\rangle_F \sim 3 \times 10^{-26} \text{cm}^3/\text{s}$ to obtain the measured abundance. As was pointed out in Ref. [56], the DM has three types of popular annihilation channels: $\tilde{\nu}_1^\tau \tilde{\nu}_1^{\tau*} \rightarrow h_s h_s, A_s A_s$, where h_s and A_s denote the singlet-dominated CP-even and CP-odd Higgs bosons, respectively, $\tilde{\nu}_1^\tau \tilde{\nu}_1^{\tau*} \rightarrow \bar{\nu}_h \nu_h$, $\tilde{\nu}_1^\tau \tilde{\nu}_1^\tau \rightarrow \nu_h \nu_h$, and $\tilde{\nu}_1^{\tau*} \tilde{\nu}_1^{\tau*} \rightarrow \bar{\nu}_h \bar{\nu}_h$, where ν_h represents any of the heavy neutrinos, and the co-annihilation with the Higgsinos. Since the singlet-dominated particles are much heavier than the DM, $\tilde{\nu}_1^\tau \tilde{\nu}_1^{\tau*} \rightarrow h_s h_s, A_s A_s$ are kinematically forbidden. The process $\tilde{\nu}_1^\tau \tilde{\nu}_1^{\tau*} \rightarrow \bar{\nu}_h \nu_h$ proceeds mainly by the s -channel exchange of h_s and the t -channel exchange of the singlino-dominated neutralino. Evidently, it is suppressed by the mediator mass. This situation applies to the channels $\tilde{\nu}_1^\tau \tilde{\nu}_1^\tau \rightarrow \nu_h \nu_h$ and $\tilde{\nu}_1^{\tau*} \tilde{\nu}_1^{\tau*} \rightarrow \bar{\nu}_h \bar{\nu}_h$. Thus, only the co-annihilation may play a crucial role. In this case, the effective annihilation rate at temperature T takes the following form [82]:

$$\sigma_{\text{eff}} = \sum_{a,b} \sigma_{ab} \frac{g_a g_b}{g_{\text{eff}}^2} (1 + \Delta_a)^{3/2} (1 + \Delta_b)^{3/2} \times \exp[-x(\Delta_a + \Delta_b)], \quad (4.1)$$

where $\sigma_{ab} = \sigma(ab \rightarrow XY)$, $a, b = \tilde{\nu}_1^\tau, \tilde{\nu}_1^{\tau*}, \tilde{\chi}_1^0, \tilde{\chi}_2^0, \tilde{\chi}_1^\pm$, X and Y denote any possible SM particles, $\Delta_i \equiv (m_i - m_{\tilde{\nu}_1^\tau})/m_{\tilde{\nu}_1^\tau}$ for $i = a, b$ represents the mass splitting between the initial particle i and $\tilde{\nu}_1^\tau$, $x \equiv m_{\tilde{\nu}_1^\tau}/T$, g_i represents the i th particle's internal degrees of freedom, with $g_{\tilde{\chi}_i^0} = 2$, $g_{\tilde{\chi}_i^\pm} = 4$, and $g_{\tilde{\nu}_1^\tau} = g_{\tilde{\nu}_1^{\tau*}} = 2$, and the effective degree of

³In this study, we take $\tilde{\nu}_1^\tau$ as a complex field by setting $B_{\nu_x} = 0$. Consequently, $\tilde{\nu}_1^{\tau*}$ also acts as a DM candidate. The ISS-NMSSM is then a two-component DM theory [56]. We add that DM physics requires non-trivial configurations in the theory's parameter space.

freedom g_{eff} is

$$g_{\text{eff}} \equiv \sum_a g_a (1 + \Delta_a)^{3/2} \exp(-x \Delta_a). \quad (4.2)$$

Since the Higgsino pair annihilation cross-section is much larger than $3 \times 10^{-26} \text{cm}^3/s$ for $\mu \simeq 100 \text{ GeV}$, these formulae indicate that, even in the case of $\sigma_{\tilde{\nu}_1^{\tau*} \tilde{\nu}_1^{\tau}} \simeq 0$ and $\sigma_{\tilde{\nu}_1^{\tau} \tilde{\nu}_1^{\tau}} = \sigma_{\tilde{\nu}_1^{\tau*} \tilde{\nu}_1^{\tau*}} \simeq 0$, the co-annihilation can explain the abundance by choosing an appropriate Δ_i s. For the samples in the last section, we verified that this is feasible by setting $Y_{\nu_\tau} \simeq 0$, $\lambda_{N_\tau} \simeq 0$ and adjusting parameters $M_{\nu_\tau}^2$ and $M_{X_\tau}^2$ to change Δ_i s. We also found that the measured abundance requires $\Delta m(\tilde{\chi}_1^0, \tilde{\nu}_1^{\tau}) \sim 5 \text{ GeV}$ for $\Delta m(\tilde{\chi}_2^0, \tilde{\chi}_1^0) \simeq 0$ and $\Delta m(\tilde{\chi}_1^\pm, \tilde{\chi}_1^0) \simeq 1 \text{ GeV}$. With the increase in $\Delta m(\tilde{\chi}_2^0, \tilde{\chi}_1^0)$ and $\Delta m(\tilde{\chi}_1^\pm, \tilde{\chi}_1^0)$, $\Delta m(\tilde{\chi}_1^0, \tilde{\nu}_1^{\tau})$ decreases monotonically to maintain the abundance.

Next, we consider the DM-nucleon scattering proceeded by the t -channel exchange of the CP-even Higgs bosons and Z boson. The spin-dependent cross section is vanishing, and the spin-independent (SI) cross section is [56]

$$\sigma_N^{\text{SI}} = \frac{1}{2} \left(\sigma_{\tilde{\nu}_1^{\tau} - N}^{\text{SI}} + \sigma_{\tilde{\nu}_1^{\tau*} - N}^{\text{SI}} \right) = \sigma_N^h + \sigma_N^Z, \quad (4.3)$$

where σ_N^h and σ_N^Z with $N = p, n$ denote the Higgs-mediated and the Z -mediated contribution, respectively. For the preferred parameters in the last section, σ_N^h and σ_N^Z are approximated by

$$\begin{aligned} \sigma_N^h / \text{cm}^2 &\simeq 4.2 \times 10^{-44} \times \frac{C_{\tilde{\nu}_1^{\tau*} \tilde{\nu}_1^{\tau} \Re[H_u^0]}^2}{m_{\tilde{\nu}_1^{\tau}}^2}, \\ \sigma_n^Z / \text{cm}^2 &= 7.4 \times 10^{-39} \times (Z_{11}^\tau)^4, \quad \sigma_n^Z / \text{cm}^2 = 4.2 \times 10^{-41} \times (Z_{11}^\tau)^4, \end{aligned} \quad (4.4)$$

where $C_{\tilde{\nu}_1^{\tau*} \tilde{\nu}_1^{\tau} \Re[H_u^0]}$ represents the coupling of the DM pair to the CP-even H_u^0 field and takes the following form:

$$C_{\tilde{\nu}_1^{\tau*} \tilde{\nu}_1^{\tau} \Re[H_u^0]} \simeq -\sqrt{2} \lambda_{N_\tau} A_{Y_{\nu_\tau}} Z_{11}^\tau Z_{12}^\tau - \lambda_{N_\tau} Y_{\nu_\tau} v_s Z_{11}^\tau Z_{13}^\tau - Y_{\nu_\tau}^2 v_u Z_{12}^\tau Z_{12}^\tau. \quad (4.5)$$

Noting that Z_{11}^τ is proportional to Y_{ν_τ} , one can conclude that the scattering is suppressed in the case of a small Y_{ν_τ} and λ_{N_τ} . This case is favored by current and future DM direct detection experiments [83].

4.2 Effect of dark matter embedding on sparticle signal at the Large Hadron Collider (LHC)

In the ISS-NMSSM, the coupling of the DM to electroweakinos are

$$\begin{aligned} g_{\tilde{\nu}_1^{\tau} \tilde{\tau} \tilde{\chi}_i^\pm} &= Y_{e_\tau} U_{i2}^* Z_{11}^\tau P_L - (g_2 V_{i1} Z_{11}^\tau - Y_{\nu_\tau} V_{i2} Z_{12}^\tau) P_R, \\ g_{\tilde{\nu}_1^{\tau} \tilde{\nu}_\tau \tilde{\chi}_i^0} &= \frac{1}{\sqrt{2}} (g_1 N_{i1} - g_2 N_{i2}) P_{11} Z_{11}^\tau P_R - (Y_{\nu_\tau} N_{i4} P_{11} Z_{12}^\tau + \lambda_{N_\tau} N_{i5} P_{13} Z_{12}^\tau) P_R \\ &\quad - (\lambda_{N_\tau} N_{i5}^* P_{12}^* Z_{13}^\tau + Y_{\nu_\tau} N_{i4}^* P_{12}^* Z_{11}^\tau) P_L, \end{aligned}$$

- For the other sparticles, their interactions with $\tilde{\nu}_1^\tau$ are weak, and thus, their decay chains do not change significantly.

Table 1 shows the details of a sample obtained in the last section, including the mass spectra and decay modes of some moderately light sparticles. In Fig. 8, we show the decay path of these sparticles to illustrate their properties further. This result indicates that the collider signature will not change after being embedded into the DM, which suggests that the constraints from the DM experiments should not be considered when studying the collider phenomenology.

Parameters	Value	Particles	Mass	Before	
M_1	143.2 GeV	$\tilde{\chi}_1^0$	110.5 GeV	Decays	Branching ratio[%]
M_2	650.0 GeV	$\tilde{\chi}_2^0$	-149.4 GeV	$\tilde{\chi}_1^0$ (LSP)	-
μ	137.6 GeV	$\tilde{\chi}_3^0$	172.3 GeV	$\tilde{\chi}_2^0 \rightarrow \tilde{\chi}_1^0 q\bar{q}/\tilde{\chi}_1^0 \ell\ell/\tilde{\chi}_1^0 \nu\nu/\tilde{\chi}_1^\pm q q'/\tilde{\chi}_1^\pm \ell\nu$	60.67 / 9.29 / 29.44 / 0.20 / 0.39
λ, κ	0.0920, 0.6081	$\tilde{\chi}_4^0$	686.7 GeV	$\tilde{\chi}_1^\pm \rightarrow \tilde{\chi}_1^0 q q'/\tilde{\chi}_1^0 \ell\nu$	65.38 / 34.72
Y_{ν_e}, λ_{N_e}	0.9565, 0.7334	$\tilde{\chi}_5^0$	1807 GeV	$\tilde{\chi}_3^0 \rightarrow \tilde{\nu}_\tau^\pm \nu/\tilde{\chi}_1^\pm q q'/\tilde{\chi}_1^\pm \ell\nu$	99.87 / 0.07 / 0.04
A_{ν_e}	387.5 GeV	$\tilde{\chi}_1^\pm$	140.3 GeV	$\tilde{\chi}_4^0 \rightarrow \tilde{\chi}_1^\pm W^\mp/\tilde{\chi}_1^0 h/\tilde{\chi}_1^0 Z/\tilde{e}_L e/\tilde{\nu}\nu$	31.91 / 14.35 / 15.31 / 15.58 / 22.56
$M_{\tilde{e}}$	332.0 GeV	$\tilde{\chi}_2^\pm$	686.9 GeV	$\tilde{\chi}_2^\pm \rightarrow \tilde{\chi}_1^\pm h/\tilde{\chi}_1^\pm Z/\tilde{\chi}_1^0 W^\pm/\tilde{\nu}\ell/\tilde{e}\nu$	14.68 / 15.44 / 31.37 / 22.60 / 15.62
$M_{\tilde{e}_c}$	883.5 GeV	\tilde{e}_L	373.5 GeV	After	
$Y_{\nu_\mu}, \lambda_{N_\mu}$	0.1701, 0.8588	\tilde{e}_R	859.9 GeV	Decays	Branching ratio[%]
A_{ν_μ}	-1943 GeV	$\tilde{\mu}_L$	767.8 GeV	$\tilde{\chi}_1^0 \rightarrow \tilde{\nu}_\tau^\pm \nu$	100.0
$M_{\tilde{\mu}}$	746.4 GeV	$\tilde{\mu}_R$	532.2 GeV	$\tilde{\chi}_2^0 \rightarrow \tilde{\chi}_1^0 q\bar{q}/\tilde{\chi}_1^0 \ell\ell/\tilde{\chi}_1^0 \nu\nu/\tilde{\chi}_1^\pm q q'/\tilde{\chi}_1^\pm \ell\nu$	57.81 / 8.85 / 32.54 / 0.20 / 0.58
$M_{\tilde{E}_\mu}$	569.2 GeV	$\tilde{\nu}_L^e$	462.5 GeV	$\tilde{\chi}_1^\pm \rightarrow \tilde{\chi}_1^0 q q'/\tilde{\chi}_1^0 \ell\nu$	65.38 / 34.72
$Y_{\nu_\tau}, \lambda_{N_\tau}$	0.0037, 0.0368	$\tilde{\nu}_R^e$	150.5 GeV	$\tilde{\chi}_3^0 \rightarrow \tilde{\nu}_\tau^\pm \nu/\tilde{\chi}_1^\pm q q'/\tilde{\chi}_1^\pm \ell\nu$	99.91 / 0.06 / 0.03
Z_{11}^T	1.112×10^{-5}	$\tilde{\nu}_X^e$	1297 GeV	$\tilde{\chi}_4^0 \rightarrow \tilde{\chi}_1^\pm W^\mp/\tilde{\chi}_1^0 h/\tilde{\chi}_1^0 Z/\tilde{e}_L e/\tilde{\nu}\nu$	31.89 / 14.34 / 15.30 / 15.57 / 22.60
$m_{\tilde{\nu}_X^e}$	110.3 GeV	$\tilde{\nu}_L^\mu$	757.2 GeV	$\tilde{\chi}_2^\pm \rightarrow \tilde{\chi}_1^\pm h/\tilde{\chi}_1^\pm Z/\tilde{\chi}_1^0 W^\pm/\tilde{\nu}\ell/\tilde{e}\nu$	14.67 / 15.44 / 31.35 / 22.64 / 15.61
Ωh^2	0.120	$\tilde{\nu}_R^\mu$	1142 GeV		
$\sigma_{\tilde{\nu}-p}^{\text{SI}}$	$5.324 \times 10^{-52} \text{ cm}^2$	$\tilde{\nu}_X^\mu$	783.5 GeV		

Table 1. Input parameters, mass spectrum, and decay modes of the sample in Fig. 8 before and after inserting τ -type sneutrino DM.

5 Constraints from LHC sparticle searches

Fig. 5 shows that to simultaneously explain Δa_e and Δa_μ , very light electroweakinos and sleptons are necessary in many samples. Generally, such light sparticles are strongly constrained by the current LHC SUSY searches.

Using the data taken at $\sqrt{s} = 7, 8$, and 13 TeV, searches for SUSY particles have been conducted for several years. First, we perform analyses at 8 and 13 TeV in **SModelS v1.2** [85, 86] to refine the samples. After this, any point that passes **SModelS** is further tested by analyses in **CheckMATE-2.0.26** [87–89]. The physical processes considered in our work are as follows:

$$\begin{aligned}
pp &\rightarrow \tilde{\chi}_i^0 \tilde{\chi}_j^\pm, & i = 2, 3, 4; & \quad j = 1, 2; \\
pp &\rightarrow \tilde{\chi}_i^\pm \tilde{\chi}_j^\mp, & i = 1, 2; & \quad j = 1, 2; \\
pp &\rightarrow \tilde{\chi}_i^0 \tilde{\chi}_j^0, & i = 2, 3, 4; & \quad j = 2, 3, 4; \\
pp &\rightarrow \tilde{\ell}_i \tilde{\ell}_i, & i = e, \mu.
\end{aligned} \tag{5.1}$$

The cross section of $\sqrt{s} = 8, 13$ TeV were normalized at the NLO using the **Prospino2** package [90]. The Monte Carlo events were generated by **MadGraph_aMC@NLO** [91, 92] with the **PYTHIA8** package [93] for parton showering and hadronization. The event files were then input into **CheckMATE** for analysis with **Delphes** [94] for detector simulation.

In addition to the analysis that has been implemented before, we added the following newly released LHC analyses to **CheckMATE**.

- **ATLAS search for chargino and neutralino production using recursive jigsaw reconstruction in three-lepton final states** [95]: This analysis is optimized for signals from $\tilde{\chi}_2^0 \tilde{\chi}_1^\pm$ production with on-shell WZ decay modes. The signal regions (SRs) are split into a low-mass region (jet-veto) and the initial state radiation (ISR) region (contains at least one energetic jet) using a variety of kinematic variables, including the dilepton invariant mass $m_{\ell\ell}$, the transverse mass m_T , and variables arising from the application of the emulated recursive jigsaw reconstruction technique. The smallness of the mass splittings lead to events with lower- p_T leptons or smaller E_T^{miss} in the final state. Cuts in the low-mass SR are designed to reduce the WZ background and the number of fake or non-prompt leptons, and cuts in the ISR region requiring large E_T^{miss} to identify events have a real E_T^{miss} source. This search is sensitive to samples with relative light winos.
- **ATLAS search for chargino and slepton pair production in two lepton final states** [84]: This analysis targets pair production of charginos and/or sleptons decaying into final states with two electrons or muons. Signal events are required to have an exactly opposite-sign (OS) signal lepton pair with a large invariant mass $m_{\ell\ell} > 100$ GeV to reduce diboson and $Z + \text{jets}$ backgrounds. SRs are separated into same-flavor and different-flavor categories with variables $m_{\ell\ell}$, the transverse mass m_{T2} [96], E_T^{miss} and E_T^{miss} significance, and the number of non- b -tagged jets. The sensitivity of this analysis to the slepton mass can reach 700 GeV, and that to the chargino mass can reach about 1 TeV (420 GeV) of the decay mode $\tilde{\chi}_1^\pm \rightarrow \tilde{\ell}\nu/\ell\tilde{\nu} \rightarrow \ell\nu\tilde{\chi}_1^0$ ($\tilde{\chi}_1^\pm \rightarrow W^\pm(\rightarrow \ell\nu)\tilde{\chi}_1^0$).
- **ATLAS search for electroweak production of supersymmetric particles with compressed mass spectra** [97]: This was optimized on a simplified model of mass-degenerated Higgsino triplets that assumed $\tilde{\chi}_2^0 \tilde{\chi}_1^\pm$ production followed by the decays $\tilde{\chi}_1^\pm \rightarrow W^* \tilde{\chi}_1^0$ and $\tilde{\chi}_2^0 \rightarrow Z^* \tilde{\chi}_1^0$. It is also sensitive to the degenerate slepton-LSP mass spectrum. The selected events have exactly two OS same-flavor leptons or one lepton plus at least one OS track, and at least one jet is required. The pre-selection requirements include the requirements that the invariant mass $m_{\ell\ell}$ is derived from the J/ψ meson mass window, that E_T^{miss} is greater than 120 GeV, and that the p_T of the leading jet is larger

than 100 GeV. After applying the pre-selection requirements, SRs are further optimized for the specific SUSY scenario into three categories: SR-E (for electroweakino recoiling against ISR), SR-VBF (electroweakino produced through vector boson fusion (VBF)), and SR-S (sleptons recoiling against ISR). A variety of kinematic variables and the recursive jigsaw reconstruction technique are used to identify the SUSY signals. Assuming Higgsino production, this search occurs at the minimum mass of $\tilde{\chi}_2^0$ at 193 GeV at a mass splitting of 9.3 GeV.

- **ATLAS search for chargino and neutralino pair production in final state with three-leptons and missing transverse momentum [98]:** This search targets chargino–neutralino pair production decaying via WZ , W^*Z^* , or Wh into three-lepton final states. This analysis uses the full LHC Run II dataset. The simplified model has an $\tilde{\chi}_2^0$ mass of up to 640 GeV for on-shell WZ decay mode with massless $\tilde{\chi}_1^0$, up to 300 GeV for the off-shell WZ decay mode, and up to 185 GeV for the Wh decay mode with an $\tilde{\chi}_1^0$ mass below 20 GeV.
- **ATLAS search for supersymmetric states with a compressed mass spectrum [99]:** This analysis uses the OS lepton pair and large E_T^{miss} , searching for the electroweakino and slepton pair production with a compressed mass spectrum. Two sets of SRs are constructed separately for the production of electroweakinos and sleptons. The electroweakino SRs require the invariant mass of the lepton pair $m_{\ell\ell}$ to be less than 60 GeV, and the slepton SRs require the transverse mass $m_{T2}^{m_\chi}$ to be greater than 100 GeV, where the hypothesized mass of the LSP m_χ is equal to 100 GeV. The most sensitive location of the mass splitting is at about 5–10 GeV. The 95% confidence level exclusion limits of the Higgsino, wino, and slepton are up to 145, 175, and 190 GeV, respectively.
- **CMS combined search for charginos and neutralinos [53]:** Various simplified models of the SUSY are used in this combined search to interpret the results. Related to our work, the simplified model scenario interpretation of $\tilde{\chi}_2^0\tilde{\chi}_1^\pm$ with decays $\tilde{\chi}_2^0 \rightarrow Z^{(*)}\tilde{\chi}_1^0/h\tilde{\chi}_1^0$ and $\tilde{\chi}_1^\pm \rightarrow W^{(*)}\tilde{\chi}_1^0$ represents the most stringent constraints from the CMS to date for electroweakino pair production. Compared with the results of individual analyses, this interpretation improves the observed limit in $\tilde{\chi}_1^\pm$ to about 650 GeV for WZ topology.
- **ATLAS search for electroweakino production in Wh final states [100]:** This was optimized on a simplified model that assumed $\tilde{\chi}_2^0\tilde{\chi}_1^\pm$ production with decay modes $\tilde{\chi}_1^\pm \rightarrow W^\pm\tilde{\chi}_1^0$ and $\tilde{\chi}_2^0 \rightarrow h\tilde{\chi}_1^0$. Signal events were selected with exactly one lepton, two b -jets requiring $100 \text{ GeV} < m_{bb} < 140 \text{ GeV}$ and $E_T^{\text{miss}} > 240 \text{ GeV}$, a transverse mass of the lepton- E_T^{miss} system m_T greater than 100 GeV, and a “contransverse mass” m_{CT} [101, 102] greater than 180 GeV. Masses

of the winos up to 740 GeV are excluded at 95% confidence level for the massless LSP.

- **CMS search in final states with two OS same-flavor leptons, jets, and missing transverse momentum [103]:** This search is sensitive to the on-shell and off-shell Z boson from BSM processes and to direct slepton production. Search regions are split into on- Z SRs, off- Z SRs, and slepton SRs via various kinematic variables, including the invariant mass of the lepton pair $m_{\ell\ell}$, M_{T2} , the scalar sum of jet p_T , the missing transverse momentum E_T^{miss} , the number of jets n_j , and the number of b -tagging jets n_b . The result interpretation using the simplified model assuming direct slepton pair production with 100% decay into dilepton final states shows that the probing limit of the slepton mass $m_{\tilde{\ell}}$ is up to 700 GeV. Certainly, this search is sensitive to the sparticles in the ISS-NMSSM interpretation of Δa_ℓ .

Appendix A shows a part of the validation table of the analyses above. We used the R values obtained from **CheckMATE** to apply the LHC constraints. Here, $R \equiv \max\{S_i/S_{i,95}^{\text{obs}}\}$ for individual analysis, in which S_i represents the simulated event number of the i_{th} SR or bin of the analysis, and $S_{i,95}^{\text{obs}}$ is the 95% confidence level upper limit of the event number in the corresponding SR or bin. The combination procedure of the CMS electroweakino search [53] was also performed though the CL_s method [104] with **RooStats** [105] using the likelihood function described previously [53].

The impacts of LHC constraints on the samples were relatively strong, as 6915 samples were excluded, and only 1396 samples survived, corresponding to a total posterior probability of 11.2%. In Fig. 9, we plot the SUSY particle mass of the surviving samples and excluded samples via a split violin plot⁴. The LHC constraints have not significantly changed the distributions of the SUSY particle mass. In Fig. 10, we plot the samples on the $m_{\tilde{\chi}_1^0} - \Delta m(\tilde{\chi}_1^0, \tilde{\chi}_1^\pm)$ plane and the $m_{\tilde{e}_L} - m_{\tilde{\mu}_L}$ plane with M_1 valued color. The detection ability of the LHC was mainly affected by the decay modes of SUSY particles.

1. For the light left-handed slepton pair production processes,
 - when $\tilde{\nu}_1^e$ is very light, as shown by the samples in Fig. 8, the dominant decay mode was $\tilde{e}_L \rightarrow W\tilde{\nu}_1^e$ (the sample in Fig. 8 for example), where $\tilde{\nu}_1^e$ contains large left-handed ingredients⁵. Such samples are difficult to detect by the current LHC experiments. In the right plane of Fig. 10 and

⁴Similar to a violin plot, the split violin plot splits the violins in half to see the difference between two sample groups. Note that the widths of both sides of the violin are fixed, so that the ratio of the two widths does not represent the relative probability or relative number.

⁵There is only one left-handed sneutrino $\tilde{\nu}_L^e$ in the MSSM or NMSSM, and its mass is slightly lighter than that of the left-handed selectron \tilde{e}_L .

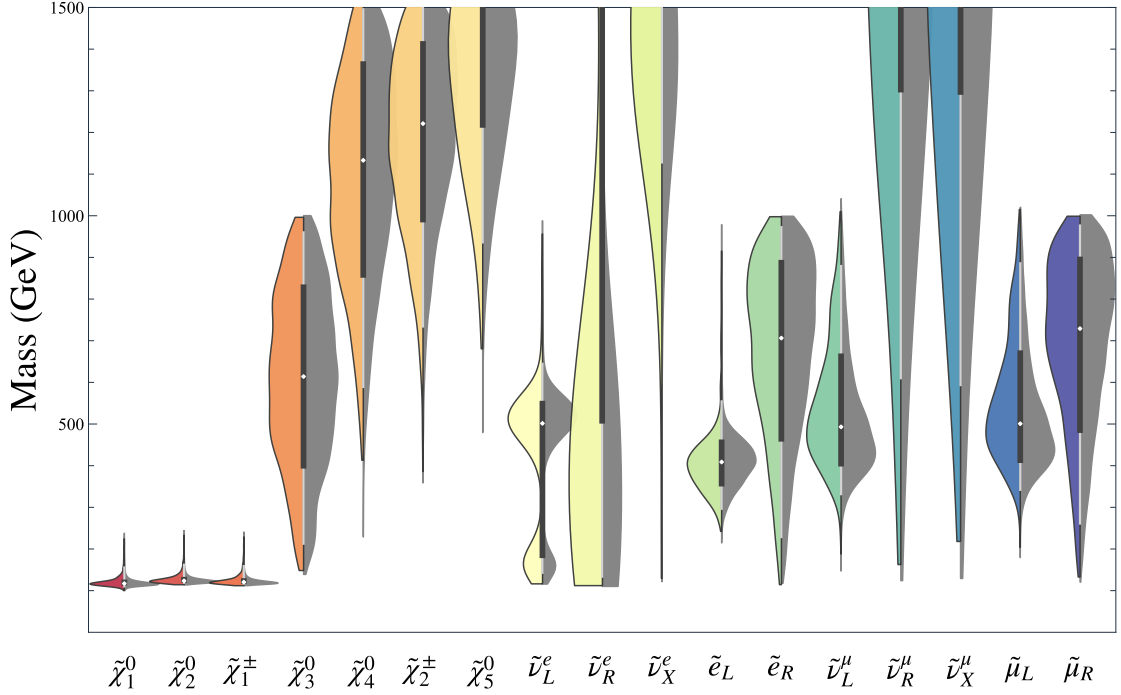


Figure 9. Split violin plot showing the SUSY particle mass distributions of samples based on the Large Hadron Collider (LHC) result. The left colorful KDEs are the mass distributions of samples that survive the LHC search results, and the right gray KDEs indicate samples excluded by the LHC results. The medians, interquartile ranges, and 95% confidence intervals are the same as those in Fig. 5.

Fig. 9, we find that the $m_{\tilde{e}_L}$ values of the surviving samples can reach 200 GeV, and such a light \tilde{e}_L is good for explaining Δa_e .

- when $|M_1|$ is lighter than $m_{\tilde{e}_L}$ or $m_{\tilde{\nu}_L}$, if $\tilde{e}_L \rightarrow W\tilde{\nu}_1^e$ is kinematically forbidden, as shown in the right panel of Fig. 6, the dominated decay mode of $\tilde{\ell}_L$ is into ℓ plus a bino-like neutralino $\tilde{\chi}^0$. In this case, the LHC slepton pair production searches provide the most sensitivity to the slepton mass. Fig. 10 shows that samples with $\mu_L < 400$ GeV and small $|M_1|$ have difficulty escaping the LHC constraints.
 - when $|M_1|$ is very large and $\tilde{\nu}_1^e$ is very heavy, the left-handed slepton will decay into $\ell\tilde{\chi}_1^0$, $\ell\tilde{\chi}_2^0$, and $\nu\tilde{\chi}_1^\pm$, as depicted in the left panel of Fig. 6. Because the decay products of $\tilde{\chi}_1^\pm$ are too soft, the LHC constraints for these samples are weaker than those in the light bino case.
2. For light right-handed slepton pair production processes, the production cross section is about 2.7 times smaller than that of left-handed slepton. The right-handed sleptons mainly decay into $\ell\tilde{\chi}_1^0$ and $\ell\tilde{\chi}_2^0$. Only a few samples contain light $\tilde{\mu}_R$ or \tilde{e}_R , so the right-handed slepton had little effect on the result.

3. For the Higgsino pair $\tilde{\chi}_2^0 \tilde{\chi}_1^\pm$ production process, the analysis in Ref. [97] provides a strong constraint on the samples featured by the small positive M_1 , as shown in the left plane of Fig. 10.
4. For the wino-dominated neutralino/chargino pair production process, the explanation of the two lepton anomalies require $M_2 > 400$ GeV, and in about more than 97% samples, the wino-like particle mass is greater than 700 GeV. Therefore, in this study, because the decay modes of the winos are more complicated, the winos did contribute to the results, but they were not the main effect.

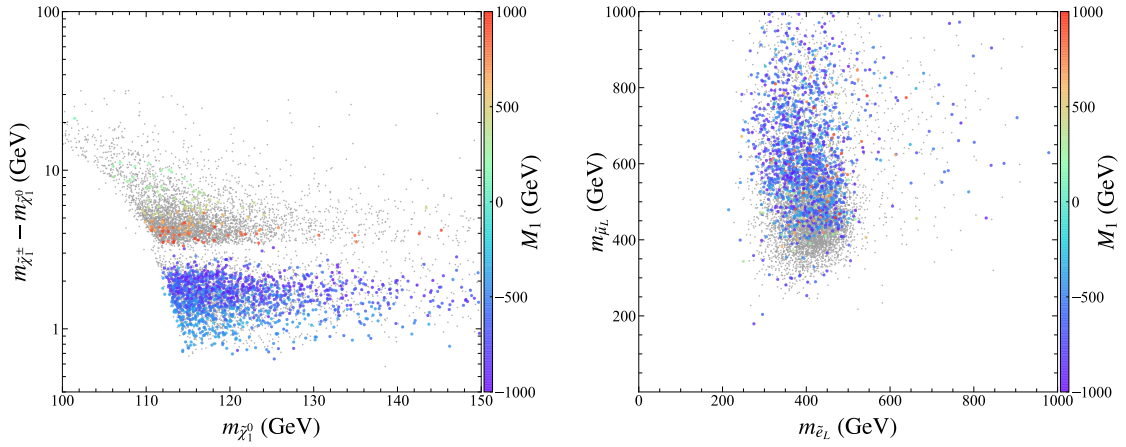


Figure 10. Samples projected on $m_{\tilde{\chi}_1^0} - \Delta m(\tilde{\chi}_1^0, \tilde{\chi}_1^\pm)$ plane and $m_{\tilde{e}_L} - m_{\tilde{\mu}_L}$ plane, where the color indicates the value of M_1 . In each plane, the gray points indicate the samples excluded by the LHC results.

In conclusion, except for some samples where \tilde{e}_L decayed to $W\tilde{\nu}_1^e$, the samples with positive M_1 were strongly restricted by the current LHC experiments. The searches for the compressed electroweakino spectrum and the searches for sleptons at the LHC are complementary in detecting samples via leptonic final states. Finally, we plot the a_e^{SUSY} and a_μ^{SUSY} values of the samples in Fig. 11. After considering the constraints from the LHC, there were still a large number of samples that could simultaneously fit Δa_e and Δa_μ at the 1σ level.

Before we conclude this section, we briefly comment that the signal of the sparticles may differ significantly from that of the NMSSM in the case of sizable Y_{ν_τ} and λ_{N_τ} [55–57]. In general, because the decay chain becomes lengthened and the signal contains at least two τ leptons, the sparticles of the ISS-NMSSM are more challenging to detect at the LHC than those of the NMSSM. We drew this conclusion by globally fitting the ISS-NMSSM with various experimental data and studying the scanned samples, similar to our previous work [56]. Therefore, we may overestimate

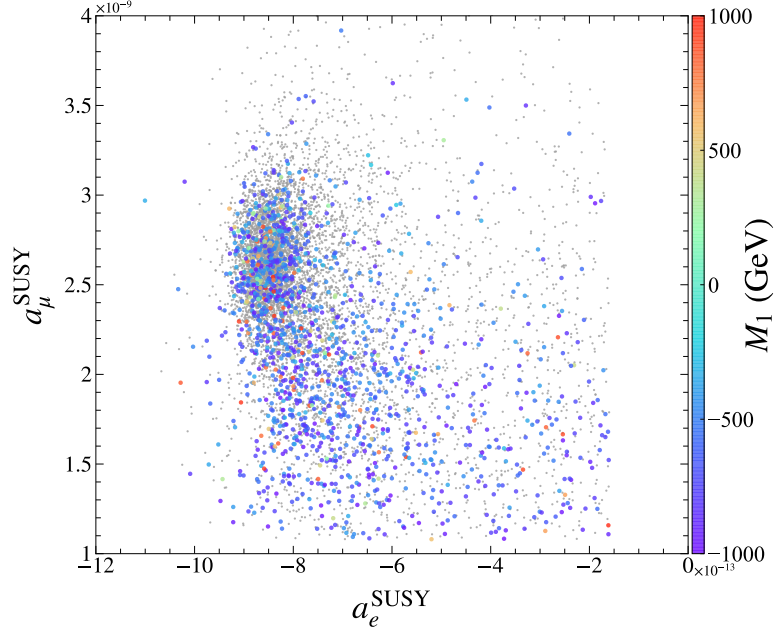


Figure 11. Similar to Fig. 10 but on $a_e^{\text{SUSY}} - a_\mu^{\text{SUSY}}$ plane with the M_1 values represented by the color.

the LHC constraints in this work, but this does not affect the main conclusion that the ISS-NMSSM can easily explain both anomalies.

6 Summary

We proposed scenarios in the ISS-NMSSM that explain both electron and muon $g - 2$ anomalies without introducing leptonic flavor violation. The results are summarized as follows:

- The HS loop induced by the neutrino Yukawa coupling Y_ν plays an important role in the explanation. The advantage of this explanation is that the sign of the HS contribution to a_ℓ can be determined by the sign of A_{ν_ℓ} , which greatly reduces the correlation between a_e and a_μ . A larger HS contribution corresponds to a light μ , which is natural for predicting m_Z .
- The features of the sparticle spectrum preferentially had large $\tan \beta$, light Higgsino $\mu \simeq 110$ GeV, and heavy wino $M_2 \gtrsim 600$ GeV. Moreover, the masses of the left-handed selectron and smuon were around 400 and 500 GeV, respectively, and the singlet Higgs-dominated particles are often heavier than 1 TeV. M_1 affects the mass splitting of Higgsino triplets and the decay mode of the sleptons.

- The mass spectrum can be introduced into a right-handed or x -field-dominated τ -type sneutrino as a proper DM candidate, which co-annihilated with Higgsinos to obtain the observed DM relic density. As indicated by the previous discussion, choosing λ_{N_τ} and Y_{ν_τ} to be less than about 0.001 can avoid the change of the LHC signal caused by the introduction of the DM, and the corresponding DM direct detection cross section is much smaller than the detection ability of the current experiment.
- The signals of the electroweakino/slepton pairs produced at the LHC are sensitive to the parameter space explaining the two anomalies, especially for a positive M_1 . However, due to the compressed mass spectrum, the insensitive decay mode of $\tilde{e}_L \rightarrow W \tilde{\nu}_1^e$, and the very heavy wino, the surviving samples can satisfy the current LHC constraints.

Acknowledgments

This work is supported by the National Natural Science Foundation of China (NNSFC) under Grant No. 11575053, No. 11905044 and No. 12075076.

A Validations of LHC analyses

This appendix verifies the correctness of our implementation of the necessary analyses in the package **CheckMATE**. For the sake of brevity, we only provide validation of the latest analyses. Table 2 shows the cut-flow validation of the analysis in Ref. [84] for chargino pair production channel. Table 3 shows the cut-flow validation for the slepton pair production channel of analysis [97]. All the cut-flow data were provided by experimental groups. The results indicate that our simulations were in good agreement with the analysis of the experimental groups.

References

- [1] J. S. Schwinger, *On Quantum electrodynamics and the magnetic moment of the electron*, *Phys. Rev.* **73** (1948) 416.
- [2] R. H. Parker, C. Yu, W. Zhong, B. Estey and H. Müller, *Measurement of the fine-structure constant as a test of the Standard Model*, *Science* **360** (2018) 191 [1812.04130].
- [3] T. Aoyama, T. Kinoshita and M. Nio, *Revised and Improved Value of the QED Tenth-Order Electron Anomalous Magnetic Moment*, *Phys. Rev. D* **97** (2018) 036001 [1712.06060].

- [4] D. Hanneke, S. Hoogerheide and G. Gabrielse, *Cavity Control of a Single-Electron Quantum Cyclotron: Measuring the Electron Magnetic Moment*, *Phys. Rev. A* **83** (2011) 052122 [[1009.4831](#)].
- [5] D. Hanneke, S. Fogwell and G. Gabrielse, *New Measurement of the Electron Magnetic Moment and the Fine Structure Constant*, *Phys. Rev. Lett.* **100** (2008) 120801 [[0801.1134](#)].
- [6] PARTICLE DATA GROUP collaboration, P. Zyla et al., *Review of Particle Physics*, *PTEP* **2020** (2020) 083C01.
- [7] T. Aoyama et al., *The anomalous magnetic moment of the muon in the Standard Model*, [2006.04822](#).
- [8] T. Aoyama, M. Hayakawa, T. Kinoshita and M. Nio, *Complete Tenth-Order QED Contribution to the Muon $g-2$* , *Phys. Rev. Lett.* **109** (2012) 111808 [[1205.5370](#)].
- [9] T. Aoyama, T. Kinoshita and M. Nio, *Theory of the Anomalous Magnetic Moment of the Electron*, *Atoms* **7** (2019) 28.
- [10] A. Czarnecki, W. J. Marciano and A. Vainshtein, *Refinements in electroweak contributions to the muon anomalous magnetic moment*, *Phys. Rev. D* **67** (2003) 073006 [[hep-ph/0212229](#)].
- [11] C. Gnendiger, D. Stöckinger and H. Stöckinger-Kim, *The electroweak contributions to $(g - 2)_\mu$ after the Higgs boson mass measurement*, *Phys. Rev. D* **88** (2013) 053005 [[1306.5546](#)].
- [12] A. Nyffeler, *Precision of a data-driven estimate of hadronic light-by-light scattering in the muon $g - 2$: Pseudoscalar-pole contribution*, *Phys. Rev. D* **94** (2016) 053006 [[1602.03398](#)].
- [13] M. Davier, A. Hoecker, B. Malaescu and Z. Zhang, *A new evaluation of the hadronic vacuum polarisation contributions to the muon anomalous magnetic moment and to $\alpha(m_Z^2)$* , *Eur. Phys. J. C* **80** (2020) 241 [[1908.00921](#)].
- [14] M. Davier, A. Hoecker, B. Malaescu and Z. Zhang, *Reevaluation of the hadronic vacuum polarisation contributions to the Standard Model predictions of the muon $g - 2$ and $\alpha(m_Z^2)$ using newest hadronic cross-section data*, *Eur. Phys. J. C* **77** (2017) 827 [[1706.09436](#)].
- [15] MUON G-2 collaboration, G. Bennett et al., *Final Report of the Muon E821 Anomalous Magnetic Moment Measurement at BNL*, *Phys. Rev. D* **73** (2006) 072003 [[hep-ex/0602035](#)].
- [16] A. Crivellin, M. Hoferichter and P. Schmidt-Wellenburg, *Combined explanations of $(g - 2)_{\mu,e}$ and implications for a large muon EDM*, *Phys. Rev. D* **98** (2018) 113002 [[1807.11484](#)].
- [17] E. J. Chun and T. Mondal, *Explaining $g - 2$ anomalies in two Higgs doublet model with vector-like leptons*, *JHEP* **11** (2020) 077 [[2009.08314](#)].

- [18] S. Jana, V. P. K., W. Rodejohann and S. Saad, *Dark matter assisted lepton anomalous magnetic moments and neutrino masses*, [2008.02377](#).
- [19] C. Arbeláez, R. Cepedello, R. M. Fonseca and M. Hirsch, *$(g - 2)$ anomalies and neutrino mass*, [2007.11007](#).
- [20] I. Doršner, S. Fajfer and S. Saad, *$\mu \rightarrow e\gamma$ selecting scalar leptoquark solutions for the $(g - 2)_{e,\mu}$ puzzles*, [2006.11624](#).
- [21] F. J. Botella, F. Cornet-Gomez and M. Nebot, *Electron and muon $g - 2$ anomalies in general flavour conserving two Higgs doublets models*, *Phys. Rev. D* **102** (2020) 035023 [[2006.01934](#)].
- [22] B. Dutta, S. Ghosh and T. Li, *Explaining $(g - 2)_{\mu,e}$, KOTO anomaly and MiniBooNE excess in an extended Higgs model with sterile neutrinos*, [2006.01319](#).
- [23] C. Hati, J. Kriewald, J. Orloff and A. Teixeira, *Anomalies in ^8Be nuclear transitions and $(g - 2)_{e,\mu}$: towards a minimal combined explanation*, *JHEP* **07** (2020) 235 [[2005.00028](#)].
- [24] J.-L. Yang, T.-F. Feng and H.-B. Zhang, *Electron and muon $(g - 2)$ in the B -LSSM*, *J. Phys. G* **47** (2020) 055004 [[2003.09781](#)].
- [25] C.-H. Chen and T. Nomura, *Electron and muon $g - 2$, radiative neutrino mass, and $\ell' \rightarrow \ell\gamma$ in a $U(1)_{e-\mu}$ model*, [2003.07638](#).
- [26] L. Calibbi, M. López-Ibañez, A. Melis and O. Vives, *Muon and electron $g - 2$ and lepton masses in flavor models*, *JHEP* **06** (2020) 087 [[2003.06633](#)].
- [27] S. Jana, V. P. K. and S. Saad, *Resolving electron and muon $g - 2$ within the 2HDM*, *Phys. Rev. D* **101** (2020) 115037 [[2003.03386](#)].
- [28] N. Haba, Y. Shimizu and T. Yamada, *Muon and Electron $g - 2$ and the Origin of Fermion Mass Hierarchy*, [2002.10230](#).
- [29] A. Cárcamo Hernández, S. King, H. Lee and S. Rowley, *Is it possible to explain the muon and electron $g - 2$ in a Z' model?*, *Phys. Rev. D* **101** (2020) 115016 [[1910.10734](#)].
- [30] M. Badziak and K. Sakurai, *Explanation of electron and muon $g - 2$ anomalies in the MSSM*, *JHEP* **10** (2019) 024 [[1908.03607](#)].
- [31] M. Bauer, M. Neubert, S. Renner, M. Schnubel and A. Thamm, *Axionlike Particles, Lepton-Flavor Violation, and a New Explanation of a_μ and a_e* , *Phys. Rev. Lett.* **124** (2020) 211803 [[1908.00008](#)].
- [32] M. Abdullah, B. Dutta, S. Ghosh and T. Li, *$(g - 2)_{\mu,e}$ and the ANITA anomalous events in a three-loop neutrino mass model*, *Phys. Rev. D* **100** (2019) 115006 [[1907.08109](#)].
- [33] M. Endo and W. Yin, *Explaining electron and muon $g - 2$ anomaly in SUSY without lepton-flavor mixings*, *JHEP* **08** (2019) 122 [[1906.08768](#)].

- [34] M. Hoferichter, *Combined explanations of $(g - 2)_\mu$, $(g - 2)_e$ and implications for a large muon EDM*, in *54th Rencontres de Moriond on Electroweak Interactions and Unified Theories*, pp. 29–34, 2019, [1905.03789](#).
- [35] B. Dutta and Y. Mimura, *Electron $g - 2$ with flavor violation in MSSM*, *Phys. Lett. B* **790** (2019) 563 [[1811.10209](#)].
- [36] H. Davoudiasl and W. J. Marciano, *Tale of two anomalies*, *Phys. Rev. D* **98** (2018) 075011 [[1806.10252](#)].
- [37] X.-F. Han, T. Li, L. Wang and Y. Zhang, *Simple interpretations of lepton anomalies in the lepton-specific inert two-Higgs-doublet model*, *Phys. Rev. D* **99** (2019) 095034 [[1812.02449](#)].
- [38] A. E. C. Hernández, S. F. King and H. Lee, *Fermion mass hierarchies from vector-like families with an extended 2HDM and a possible explanation for the electron and muon anomalous magnetic moments*, [2101.05819](#).
- [39] L. Delle Rose, S. Khalil and S. Moretti, *Explaining electron and muon $g - 2$ anomalies in an Aligned 2-Higgs Doublet Model with Right-Handed Neutrinos*, [2012.06911](#).
- [40] S.-P. Li, X.-Q. Li, Y.-Y. Li, Y.-D. Yang and X. Zhang, *Power-aligned 2HDM: a correlative perspective on $(g - 2)_{e,\mu}$* , *JHEP* **01** (2021) 034 [[2010.02799](#)].
- [41] C.-K. Chua, *Data-driven study of the implications of anomalous magnetic moments and lepton flavor violating processes of e , μ and τ* , *Phys. Rev. D* **102** (2020) 055022 [[2004.11031](#)].
- [42] M. Endo, S. Iguro and T. Kitahara, *Probing $e\mu$ flavor-violating ALP at Belle II*, *JHEP* **06** (2020) 040 [[2002.05948](#)].
- [43] G. Hiller, C. Hormigos-Feliu, D. F. Litim and T. Steudtner, *Anomalous magnetic moments from asymptotic safety*, *Phys. Rev. D* **102** (2020) 071901 [[1910.14062](#)].
- [44] S. Gardner and X. Yan, *Light scalars with lepton number to solve the $(g - 2)_e$ anomaly*, *Phys. Rev. D* **102** (2020) 075016 [[1907.12571](#)].
- [45] J. Aebischer, W. Dekens, E. E. Jenkins, A. V. Manohar, D. Sengupta and P. Stoffer, *Effective field theory interpretation of lepton magnetic and electric dipole moments*, [2102.08954](#).
- [46] A. Bodas, R. Coy and S. J. D. King, *Solving the electron and muon $g - 2$ anomalies in Z' models*, [2102.07781](#).
- [47] G. Giudice, P. Paradisi and M. Passera, *Testing new physics with the electron $g-2$* , *JHEP* **11** (2012) 113 [[1208.6583](#)].
- [48] H. Baer, V. Barger, S. Salam, D. Sengupta and X. Tata, *The LHC higgsino discovery plane for present and future SUSY searches*, [2007.09252](#).
- [49] J. Cao, Y. He, L. Shang, Y. Zhang and P. Zhu, *Current status of a natural NMSSM*

- in light of LHC 13 TeV data and XENON-1T results, *Phys. Rev. D* **99** (2019) 075020 [[1810.09143](#)].
- [50] S. Dimopoulos and G. Giudice, *Naturalness constraints in supersymmetric theories with nonuniversal soft terms*, *Phys. Lett. B* **357** (1995) 573 [[hep-ph/9507282](#)].
 - [51] G. Giudice and R. Rattazzi, *Living Dangerously with Low-Energy Supersymmetry*, *Nucl. Phys. B* **757** (2006) 19 [[hep-ph/0606105](#)].
 - [52] H. Baer, V. Barger, P. Huang and X. Tata, *Natural Supersymmetry: LHC, dark matter and ILC searches*, *JHEP* **05** (2012) 109 [[1203.5539](#)].
 - [53] CMS collaboration, A. Sirunyan et al., *Combined search for electroweak production of charginos and neutralinos in proton-proton collisions at $\sqrt{s} = 13$ TeV*, *JHEP* **03** (2018) 160 [[1801.03957](#)].
 - [54] J. Cao, J. Lian, L. Meng, Y. Yue and P. Zhu, *Anomalous muon magnetic moment in the inverse seesaw extended next-to-minimal supersymmetric standard model*, *Phys. Rev. D* **101** (2020) 095009 [[1912.10225](#)].
 - [55] J. Cao, L. Meng, Y. Yue, H. Zhou and P. Zhu, *Suppressing the scattering of WIMP dark matter and nucleons in supersymmetric theories*, *Phys. Rev. D* **101** (2020) 075003 [[1910.14317](#)].
 - [56] J. Cao, Y. He, Y. Pan, Y. Yue, H. Zhou and P. Zhu, *Impact of leptonic unitarity and dark matter direct detection experiments on the NMSSM with inverse seesaw mechanism*, [1903.01124](#).
 - [57] J. Cao, X. Guo, Y. He, L. Shang and Y. Yue, *Sneutrino DM in the NMSSM with inverse seesaw mechanism*, *JHEP* **10** (2017) 044 [[1707.09626](#)].
 - [58] E. Arganda, M. J. Herrero, X. Marcano and C. Weiland, *Imprints of massive inverse seesaw model neutrinos in lepton flavor violating Higgs boson decays*, *Phys. Rev. D* **91** (2015) 015001 [[1405.4300](#)].
 - [59] J. Baglio and C. Weiland, *The triple Higgs coupling: A new probe of low-scale seesaw models*, *JHEP* **04** (2017) 038 [[1612.06403](#)].
 - [60] U. Ellwanger, C. Hugonie and A. M. Teixeira, *The Next-to-Minimal Supersymmetric Standard Model*, *Phys. Rept.* **496** (2010) 1 [[0910.1785](#)].
 - [61] S. P. Martin and J. D. Wells, *Muon Anomalous Magnetic Dipole Moment in Supersymmetric Theories*, *Phys. Rev. D* **64** (2001) 035003 [[hep-ph/0103067](#)].
 - [62] F. Feroz, M. Hobson and M. Bridges, *MultiNest: an efficient and robust Bayesian inference tool for cosmology and particle physics*, *Mon. Not. Roy. Astron. Soc.* **398** (2009) 1601 [[0809.3437](#)].
 - [63] F. Feroz, M. Hobson, E. Cameron and A. Pettitt, *Importance Nested Sampling and the MultiNest Algorithm*, *Open J. Astrophys.* **2** (2019) 10 [[1306.2144](#)].
 - [64] P. Bechtle, S. Heinemeyer, O. Stål, T. Stefaniak and G. Weiglein, *HiggsSignals*:

- Confronting arbitrary Higgs sectors with measurements at the Tevatron and the LHC*, *Eur. Phys. J. C* **74** (2014) 2711 [[1305.1933](#)].
- [65] O. Stål and T. Stefaniak, *Constraining extended Higgs sectors with HiggsSignals*, *PoS EPS-HEP2013* (2013) 314 [[1310.4039](#)].
 - [66] P. Bechtle, S. Heinemeyer, O. Stål, T. Stefaniak and G. Weiglein, *Probing the Standard Model with Higgs signal rates from the Tevatron, the LHC and a future ILC*, *JHEP* **11** (2014) 039 [[1403.1582](#)].
 - [67] P. Bechtle, O. Brein, S. Heinemeyer, O. Stål, T. Stefaniak, G. Weiglein et al., *HiggsBounds – 4: Improved Tests of Extended Higgs Sectors against Exclusion Bounds from LEP, the Tevatron and the LHC*, *Eur. Phys. J. C* **74** (2014) 2693 [[1311.0055](#)].
 - [68] F. Staub, *Exploring new models in all detail with SARAH*, *Adv. High Energy Phys.* **2015** (2015) 840780 [[1503.04200](#)].
 - [69] A. Vicente, *Computer tools in particle physics*, [1507.06349](#).
 - [70] W. Porod, *SPheno, a program for calculating supersymmetric spectra, SUSY particle decays and SUSY particle production at e^+e^- colliders*, *Comput. Phys. Commun.* **153** (2003) 275 [[hep-ph/0301101](#)].
 - [71] W. Porod and F. Staub, *SPheno 3.1: Extensions including flavour, CP-phases and models beyond the MSSM*, *Comput. Phys. Commun.* **183** (2012) 2458 [[1104.1573](#)].
 - [72] W. Porod, F. Staub and A. Vicente, *A Flavor Kit for BSM models*, *Eur. Phys. J. C* **74** (2014) 2992 [[1405.1434](#)].
 - [73] J. Camargo-Molina, B. O’Leary, W. Porod and F. Staub, *Vevacious: A Tool For Finding The Global Minima Of One-Loop Effective Potentials With Many Scalars*, *Eur. Phys. J. C* **73** (2013) 2588 [[1307.1477](#)].
 - [74] J. Camargo-Molina, B. Garbrecht, B. O’Leary, W. Porod and F. Staub, *Constraining the Natural MSSM through tunneling to color-breaking vacua at zero and non-zero temperature*, *Phys. Lett. B* **737** (2014) 156 [[1405.7376](#)].
 - [75] C. L. Wainwright, *CosmoTransitions: Computing Cosmological Phase Transition Temperatures and Bubble Profiles with Multiple Fields*, *Comput. Phys. Commun.* **183** (2012) 2006 [[1109.4189](#)].
 - [76] J. L. Hintze and R. D. Nelson, *Violin plots: a box plot-density trace synergism*, *The American Statistician* **52** (1998) 181.
 - [77] H. Baer, V. Barger and H. Serce, *SUSY under siege from direct and indirect WIMP detection experiments*, *Phys. Rev. D* **94** (2016) 115019 [[1609.06735](#)].
 - [78] GAMBIT collaboration, P. Athron et al., *Global fits of GUT-scale SUSY models with GAMBIT*, *Eur. Phys. J. C* **77** (2017) 824 [[1705.07935](#)].
 - [79] S. Profumo, T. Stefaniak and L. Stephenson Haskins, *The Not-So-Well Tempered Neutralino*, *Phys. Rev. D* **96** (2017) 055018 [[1706.08537](#)].

- [80] E. Bagnaschi et al., *Likelihood Analysis of the pMSSM11 in Light of LHC 13-TeV Data*, *Eur. Phys. J. C* **78** (2018) 256 [[1710.11091](#)].
- [81] K. Kowalska and E. M. Sessolo, *The discreet charm of higgsino dark matter - a pocket review*, *Adv. High Energy Phys.* **2018** (2018) 6828560 [[1802.04097](#)].
- [82] K. Griest and D. Seckel, *Three exceptions in the calculation of relic abundances*, *Phys. Rev. D* **43** (1991) 3191.
- [83] M. Benabderrahmane, *Latest results from the XENON1T experiment*, *J. Phys. Conf. Ser.* **1258** (2019) 012009.
- [84] ATLAS collaboration, G. Aad et al., *Search for electroweak production of charginos and sleptons decaying into final states with two leptons and missing transverse momentum in $\sqrt{s} = 13$ TeV pp collisions using the ATLAS detector*, *Eur. Phys. J. C* **80** (2020) 123 [[1908.08215](#)].
- [85] S. Kraml, S. Kulkarni, U. Laa, A. Lessa, W. Magerl, D. Proschofsky-Spindler et al., *SModelS: a tool for interpreting simplified-model results from the LHC and its application to supersymmetry*, *Eur. Phys. J. C* **74** (2014) 2868 [[1312.4175](#)].
- [86] F. Ambrogio et al., *SModelS v1.2: long-lived particles, combination of signal regions, and other novelties*, *Comput. Phys. Commun.* **251** (2020) 106848 [[1811.10624](#)].
- [87] M. Drees, H. Dreiner, D. Schmeier, J. Tattersall and J. S. Kim, *CheckMATE: Confronting your Favourite New Physics Model with LHC Data*, *Comput. Phys. Commun.* **187** (2015) 227 [[1312.2591](#)].
- [88] D. Dercks, N. Desai, J. S. Kim, K. Rolbiecki, J. Tattersall and T. Weber, *CheckMATE 2: From the model to the limit*, *Comput. Phys. Commun.* **221** (2017) 383 [[1611.09856](#)].
- [89] J. S. Kim, D. Schmeier, J. Tattersall and K. Rolbiecki, *A framework to create customised LHC analyses within CheckMATE*, *Comput. Phys. Commun.* **196** (2015) 535 [[1503.01123](#)].
- [90] W. Beenakker, R. Hopker and M. Spira, *PROSPINO: A Program for the production of supersymmetric particles in next-to-leading order QCD*, [hep-ph/9611232](#).
- [91] J. Alwall, M. Herquet, F. Maltoni, O. Mattelaer and T. Stelzer, *MadGraph 5 : Going Beyond*, *JHEP* **06** (2011) 128 [[1106.0522](#)].
- [92] E. Conte, B. Fuks and G. Serret, *MadAnalysis 5, A User-Friendly Framework for Collider Phenomenology*, *Comput. Phys. Commun.* **184** (2013) 222 [[1206.1599](#)].
- [93] T. Sjöstrand, S. Ask, J. R. Christiansen, R. Corke, N. Desai, P. Ilten et al., *An introduction to PYTHIA 8.2*, *Comput. Phys. Commun.* **191** (2015) 159 [[1410.3012](#)].
- [94] DELPHES 3 collaboration, J. de Favereau, C. Delaere, P. Demin, A. Giammanco, V. Lemaître, A. Mertens et al., *DELPHES 3, A modular framework for fast simulation of a generic collider experiment*, *JHEP* **02** (2014) 057 [[1307.6346](#)].

- [95] ATLAS collaboration, G. Aad et al., *Search for chargino-neutralino production with mass splittings near the electroweak scale in three-lepton final states in $\sqrt{s}=13$ TeV pp collisions with the ATLAS detector*, *Phys. Rev. D* **101** (2020) 072001 [[1912.08479](#)].
- [96] A. Barr, C. Lester and P. Stephens, *$m(T_2)$: The Truth behind the glamour*, *J. Phys. G* **29** (2003) 2343 [[hep-ph/0304226](#)].
- [97] ATLAS collaboration, G. Aad et al., *Searches for electroweak production of supersymmetric particles with compressed mass spectra in $\sqrt{s} = 13$ TeV pp collisions with the ATLAS detector*, *Phys. Rev. D* **101** (2020) 052005 [[1911.12606](#)].
- [98] ATLAS collaboration, *Search for chargino-neutralino pair production in final states with three leptons and missing transverse momentum in $\sqrt{s} = 13$ TeV p-p collisions with the ATLAS detector*, .
- [99] ATLAS collaboration, M. Aaboud et al., *Search for electroweak production of supersymmetric states in scenarios with compressed mass spectra at $\sqrt{s} = 13$ TeV with the ATLAS detector*, *Phys. Rev. D* **97** (2018) 052010 [[1712.08119](#)].
- [100] ATLAS collaboration, G. Aad et al., *Search for direct production of electroweakinos in final states with one lepton, missing transverse momentum and a Higgs boson decaying into two b-jets in pp collisions at $\sqrt{s} = 13$ TeV with the ATLAS detector*, *Eur. Phys. J. C* **80** (2020) 691 [[1909.09226](#)].
- [101] D. R. Tovey, *On measuring the masses of pair-produced semi-invisibly decaying particles at hadron colliders*, *JHEP* **04** (2008) 034 [[0802.2879](#)].
- [102] G. Polesello and D. R. Tovey, *Supersymmetric particle mass measurement with the boost-corrected contranverse mass*, *JHEP* **03** (2010) 030 [[0910.0174](#)].
- [103] CMS collaboration, *Search for physics beyond the standard model in final states with two opposite-charge same-flavor leptons, jets, and missing transverse momentum in pp collisions at 13 TeV*, .
- [104] A. L. Read, *Presentation of search results: The $CL(s)$ technique*, *J. Phys. G* **28** (2002) 2693.
- [105] ROOSTATS TEAM collaboration, G. Schott, *RooStats for Searches*, in *PHYSTAT 2011*, (Geneva), pp. 199–208, CERN, 2011, [1203.1547](#), [DOI](#).

Table 2. Cut-flow validation of ATLAS analysis [84] for mass point $m(\tilde{\chi}_1^\pm, \tilde{\chi}_1^0) = (300, 50)$ GeV in search channel of $\tilde{\chi}_1^\pm \tilde{\chi}_1^\mp$ production with W -boson-mediated decays. The yields in “Baseline” of “CheckMATE” are normalized to “Baseline” of “ATLAS”. “Efficiency” is defined as the ratio of the event number passing through the cut-flow to the event number of the previous event.

Process Point $m(\tilde{\chi}_1^\pm, \tilde{\chi}_1^0)$ Generated events	$pp \rightarrow \tilde{\chi}_1^+ \tilde{\chi}_1^-, \tilde{\chi}_1^\pm \rightarrow W^\pm \tilde{\chi}_1^0$ (300, 50) GeV 500,000			
Selection	ATLAS		CheckMATE	
	events	efficiency	events	efficiency
Preselection				
Baseline	1144.0	...	1144.0	...
Trigger	793.0	69.3%	766.0	66.9%
OS signal leptons	661.0	83.4%	725.1	94.7%
$p_T^{\ell_1, \ell_2} > 25$ GeV	565.0	85.5%	548.6	75.7%
$m_{\ell\ell} > 25$ GeV	559.0	98.9%	542.5	98.9%
$n_{b\text{-jet}} = 0$	526.0	94.1%	507.8	93.6%
SR-DF-0J				
Different flavor & $n_{\text{jets}} = 0$	122.7	23.3%	134.3	26.4%
$m_{\ell\ell} > 100$ GeV	94.2	76.8%	96.1	71.6%
$E_T^{\text{miss}} > 110$ GeV	46.5	49.4%	43.4	45.2%
E_T^{miss} significance > 10	42.2	90.8%	39.5	90.9%
$m_{T2} > 100$ GeV	26.4	62.6%	26.3	66.7%
SR-DF-1J				
Different flavor & $n_{\text{jets}} = 1$	81.9	15.6%	84.6	16.7%
$m_{\ell\ell} > 100$ GeV	62.3	76.1%	57.7	68.2%
$E_T^{\text{miss}} > 110$ GeV	33.8	54.3%	30.3	52.5%
E_T^{miss} significance > 10	27.2	80.5%	28.2	93.3%
$m_{T2} > 100$ GeV	15.3	56.3%	14.7	52.0%
SR-SF-0J				
Same flavor & $n_{\text{jets}} = 0$	138.7	26.4%	111.1	21.9%
$m_{\ell\ell} > 121.2$ GeV	92.4	75.3%	74.2	66.8%
$E_T^{\text{miss}} > 110$ GeV	47.1	50.0%	40.4	54.5%
E_T^{miss} significance > 10	42.9	92.3%	35.9	88.7%
$m_{T2} > 100$ GeV	25.4	61.9%	21.8	60.7%
SR-SF-1J				
Same flavor & $n_{\text{jets}} = 1$	88.8	16.9%	82.4	16.2%
$m_{\ell\ell} > 121.2$ GeV	58.9	66.3%	48.0	58.3%
$E_T^{\text{miss}} > 110$ GeV	32.6	55.4%	25.4	52.8%
E_T^{miss} significance > 10	26.9	82.5%	24.9	98.0%
$m_{T2} > 100$ GeV	14.0	52.0%	11.2	45.1%

Table 3. Similar to Table 2, but for the cut-flow validation of ATLAS analysis [95] in the search channel of the slepton pair production with mass point $m(\tilde{\ell}, \tilde{\chi}_1^0) = (150, 140)$ GeV.

Process	$pp \rightarrow \tilde{\ell}\tilde{\ell}, \tilde{\ell} \rightarrow \ell\tilde{\chi}_1^0$			
Point	$m_{\tilde{\ell}} = 150$ GeV; $m_{\tilde{\chi}_1^0} = 140$ GeV			
Generated events	100,000			
Selection	ATLAS		CheckMATE	
	events	efficiency	events	efficiency
E_T^{miss} trigger	2355.37	...	2355.37	...
3rd lepton veto	1014.55	43.1%	1079.07	45.8%
$3 \text{ GeV} < m_{\ell\ell} < 3.2 \text{ GeV}$ veto	1013.21	99.9%	1077.69	99.9%
Lepton author 16 veto	1009.48	99.6%	1077.69	100.0%
$\min(\Delta\phi(\text{jet}, p_T^{\text{miss}})) > 0.4$	970.36	96.1%	1049.11	97.4%
$\Delta\phi(j_1, p_T^{\text{miss}}) > 2.0$	961.15	99.1%	1027.05	97.9%
lepton truth matching	958.99	99.8%	1027.05	100.0%
$1 \text{ GeV} < m_{\ell\ell} < 60 \text{ GeV}$	827.86	86.3%	883.55	86.0%
$\Delta R_{ee} > 0.3, \Delta R_{\mu\mu} > 0.05, \Delta R_{e\mu} > 0.2$	826.19	99.8%	883.48	99.9%
$p_T^{\ell_1} > 5 \text{ GeV}$	823.70	99.7%	880.95	99.7%
$n_{\text{jets}} \geq 1$	810.59	98.4%	880.95	100.0%
$p_T^{j_1} > 100 \text{ GeV}$	705.86	87.1%	702.58	79.8%
$n_{b\text{-jets}} = 0$	611.05	86.6%	643.78	91.6%
$m_{\tau\tau} < 0$ or $m_{\tau\tau} > 160 \text{ GeV}$	533.29	87.3%	569.78	88.5%
same flavor	532.33	99.8%	569.01	99.9%
SR-highMass				
$E_T^{\text{miss}} > 200 \text{ GeV}$	229.81	43.2%	265.83	46.7%
$\max(0.85, 0.98 - 0.02 \times m_{T_2}^{100}) < R_{\text{ISR}} < 1.0$	160.30	69.8%	165.78	62.4%
$p_T^{\ell_2} > \min(20.0, 2.5 + 2.5 \times (m_{T_2}^{100} - 100))$	70.71	44.1%	72.51	43.7%
$m_{T_2}^{100} < 140 \text{ GeV}$	70.71	100.0%	72.51	100.0%
$m_{T_2}^{100} < 130 \text{ GeV}$	70.71	100.0%	72.51	100.0%
$m_{T_2}^{100} < 120 \text{ GeV}$	70.71	100.0%	72.31	99.7%
$m_{T_2}^{100} < 110 \text{ GeV}$	70.71	100.0%	72.23	99.9%
$m_{T_2}^{100} < 105 \text{ GeV}$	53.72	76.0%	57.10	79.1%
$m_{T_2}^{100} < 102 \text{ GeV}$	20.21	37.6%	23.77	41.6%
$m_{T_2}^{100} < 101 \text{ GeV}$	9.38	46.4%	9.90	41.6%
$m_{T_2}^{100} < 100.5 \text{ GeV}$	4.68	49.9%	4.86	49.1%
SR-lowMass				
$150 \text{ GeV} < E_T^{\text{miss}} < 200 \text{ GeV}$	146.36	27.5%	167.63	29.5%
$0.8 < R_{\text{ISR}} < 1.0$	107.82	73.7%	93.17	55.6%
$p_T^{\ell_2} > \min(15.0, 7.5 + 0.75 \times (m_{T_2}^{100} - 100))$	52.74	48.9%	42.29	45.4%
$m_{T_2}^{100} < 140 \text{ GeV}$	52.74	100.0%	42.29	100.0%
$m_{T_2}^{100} < 130 \text{ GeV}$	52.74	100.0%	42.29	100.0%
$m_{T_2}^{100} < 120 \text{ GeV}$	52.74	100.0%	42.29	100.0%
$m_{T_2}^{100} < 110 \text{ GeV}$	52.64	99.8%	41.65	98.5%
$m_{T_2}^{100} < 105 \text{ GeV}$	38.05	72.3%	29.09	69.9%
$m_{T_2}^{100} < 102 \text{ GeV}$	16.66	43.8%	11.24	38.6%
$m_{T_2}^{100} < 101 \text{ GeV}$	8.70	52.2%	5.60	49.8%
$m_{T_2}^{100} < 100.5 \text{ GeV}$	4.39	50.5%	2.29	40.9%